OH-initiated atmospheric degradation of hydroxyalkyl hydroperoxides: mechanism, kinetics, and structure-activity relationship

Long Chen,[1,2] Yu Huang, *[1,2] Yonggang Xue, [1,2] Zhihui Jia,[3] Wenliang Wang[4]

[1] *State Key Lab of Loess and Quaternary Geology (SKLLQG), Institute of Earth Environment, Chinese Academy of Sciences (CAS), Xi'an, 710061, China*

[2] *CAS Center for Excellence in Quaternary Science and Global Change, Xi'an, 710061, China*

[3] *School of Materials Science and Engineering, Shaanxi Normal University, Xi'an, Shaanxi, 710119, China*

[4] *School of Chemistry and Chemical Engineering, Key Laboratory for Macromolecular Science of Shaanxi Province, Shaanxi Normal University, Xi'an, Shaanxi, 710119, China*

Submitted to *Atmospheric Chemistry & Physics*

*Corresponding author:

Prof. Yu Huang, E-mail address: huangyu@ieecas.cn

Abstract:

Hydroxyalkyl hydroperoxides (HHPs), formed in the reactions of Criegee intermediates (CIs) with water vapour, play essential roles in the formation of secondary organic aerosol (SOA) under atmospheric conditions. However, the transformation mechanism for OH-initiated oxidation of HHPs is remain incompletely understood. Herein, the quantum chemical and kinetics modeling methods are applied to insight into the detailed mechanisms of OH-initiated oxidation of distinct HHPs ($HOCH_2OOH$, $HOCH(CH_3)OOH$ and $HOC(CH_3)_2OOH$) formed from the reactions of CH_2OO, *anti*-CH_3CHOO and $(CH_3)_2COO$) with water vapor. The calculations show that the dominant pathway is the H-abstraction from the -OOH group in the initiation reactions of OH radical with $HOCH_2OOH$ and $HOC(CH_3)_2OOH$. H-abstraction from -CH group is competitive with that from the -OOH group in the reaction of OH radical with $HOCH(CH_3)OOH$. The barrier of H-abstraction from the -OOH group is slightly increased as the number of methyl group is increased. In pristine environments, the self-reaction of RO_2 radical initially produces tetroxide intermediate via an oxygen-to-oxygen coupling, then it decomposes into propagation and termination products through the asymmetric two-step O-O bond scission, in which the rate-limiting step is the first O-O bond cleavage. The barrier height of distinct RO_2 radicals reactions with HO_2 radical is independent on the number of methyl substitution. In urban environments, reaction with O_2 forming formic acid and HO_2 radical is the dominant removal pathway for $HOCH_2O$ radical formed from the reaction of $HOCH_2OO$ radical with NO. The β-site C-C bond scission is the dominate pathway in the dissociation of $HOCH(CH_3)O$ and $HOC(CH_3)_2O$ radicals formed from the $HOCH(CH_3)OO \cdot + NO$ and $HOC(CH_3)_2OO \cdot + NO$ reactions. These new findings are expected to deepen our current understanding for the photochemical oxidation of hydroperoxides under realistic atmospheric conditions.

1. Introduction

Hydroxyalkyl hydroperoxides (HHPs), formed in the reactions of Criegee intermediates (CIs) with water vapour and in the initiation OH-addition with subsequent HO_2-termination reactions, play important roles in the formation of secondary organic aerosol (SOA) (Qiu et al., 2019; Kumar et al., 2014). The CIs formed from the ozonolysis of alkenes are characterized by high reactivity and excess energies, which can proceed either prompt unimolecular decay to OH radical or, after collisional stabilization, bimolecular reactions with various trance gases like SO_2, NO_2 and H_2O to produce sulfate, nitrate and SOA, thereby influencing air quality and human health (Lester and Klippenstein, 2018; Chen et al., 2017, 2019; Liu et al., 2019; Chhantyal-Pun et al., 2017; Anglada and Solé, 2016; Gong and Chen, 2021). Among these reactions, the bimolecular reaction of CIs with water is thought to be the dominant chemical sink because its concentration (1.3-8.3 $\times 10^{17}$ molecules cm^{-3}) is several orders of magnitude greater than those of SO_2 and NO_2 (~ 10^{12} molecules cm^{-3}) in the atmosphere (Huang et al., 2015; Khan et al., 2018; Taatjes et al., 2013, 2017). The primary products of CIs reactivity toward water are highly oxygenated HHPs that are difficult to detect and identify by using the available analytical techniques due to their thermally instability (Qiu et al., 2019; Anglada and Solé, 2016; Chao et al., 2015; Chen et al., 2016a; Ryzhkov and Ariya, 2003).

HHPs, due to the presence of both hydroxyl and perhydroxy moieties, have relatively low volatility contributing substantially to the formation of SOA (Qiu et al., 2019). The atmospheric degradation of HHPs initiated by OH radical is expected to be one of the dominant loss processes because OH radical is the most powerful oxidizing agent (Gligorovski et al., 2015; Allen et al., 2018). Reaction with OH radical includes three possible H-abstraction channels: (a) the alkyl hydrogen, (b) the -OH hydrogen, and (c) the -OOH hydrogen, which is followed by further reactions to generate organic peroxy radicals (RO_2) as reactive intermediates (Allen et al., 2018). Based on our current mechanistic understanding, RO_2 radicals have three possible channels in pristine environments: (1) they can proceed self- and cross-reactions resulting in

86   formation of alkoxy radical RO, alcohol, carbonyl, accretion products (Berndt et al.,

87   2018; Zhang et al., 2012; Valiev et al., 2019); (2) they can react with HO_2 radical

88   leading to the formation of closed-shell hydroperoxide (ROOH), RO ; OH radical,

89   etc.; (Dillon and Crowley, 2008; Iyer et al., 2018) (3) they can undergo autoxidation

90   via intramolecular H-shift and alternating O_2-addition steps producing highly

91   oxygenated organic molecules (HOMs), which have been identified as the low

92   volatility compounds that contribute to the formation of SOA (Crounse et al., 2013;

93   Jokinen et al., 2014; Wang et al., 2018; Ehn et al., 2014; Iyer et al., 2021). In urban

94   environments, RO_2 radicals can react with NO_x generating peroxynitrate (RO_2NO_2),

95   organic nitrate ($RONO_2$), RO ·and other SOA precursors (Wang et al., 2017; Xu et al.,

96   2014, 2020; Ma et al., 2021). The relative importance of distinct pathways depends

97   strongly on the nature of RO_2 radicals and the concentrations of coreactants.

98   Hydroxymethyl hydroperoxide (HMHP, $HOCH_2OOH$), the simplest HHPs from

99   the ozonolysis of ethene in the presence of water, is observed in significant abundance

100 in the atmosphere (Allen et al., 2018). The measured concentration of HMHP is varied

101 considerably depending on the location, season and altitude, and its concentration is

102 measured to be up to 5 ppbv in forested regions (Allen et al., 2018; Francisco and

103 Eisfeld, 2009). Recently, the concentration of HMHP was measured during the

104 summer 2013 in the southeastern United States, and found that the average mixing

105 ratio of HMHP is 0.25 ppbv with a maximum of 4.0 ppbv in the boundary layer(Allen

106 et al., 2018). A recent experimental study by Allen et al. (2018) conducted the

107 OH-initiated oxidation of HMHP in an environmental chamber and simulated the

108 impact of HMHP oxidation on the global formic acid concentrations using the

109 chemical transport model GEOS-Chem. It was found that H-abstraction from the

110 methyl group of HMHP results in formic acid, and it contributes to the global formic

111 acid production about 1.7 Tg yr^{-1}. Francisco and Eisfeld (2009) by employing *ab*

112 *initio* CCSD(T)//MP2 methods, studied the atmospheric oxidation mechanism of

113 HMHP initiated by OH radical, arriving at the same conclusion that the degradation of

114 HMHP could be a new source of formic acid in the atmosphere. Additionally, the

115 unimolecular decomposition of HMHP is another important removal process in the

116 atmosphere. Chen et al. (2016b) found that the formation of CH_2O and H_2O_2 is more

117 preferable than that of the production of HCOOH and H_2O. Kumar et al. (2014)

118 obtained the same conclusion that the aldehyde- or ketone-forming pathway is

119 kinetically favored over that the carboxylic acid-forming channel in the unimolecular

120 decomposition of a variety of HHPs. All the above milestone investigations offer very

121 useful information for understanding the decomposition of HHPs in the gas phase.

122 However, to the best of our knowledge, there is a few studies on the subsequent

123 transformations of the resulting H-abstraction products formed from the OH-initiated

124 oxidation of larger HHPs. And the effect of the size and number of substituents on the

125 rates and outcomes of SOA precursors (e.g. ROOR, HOMs) is uncertain up to now.

126 Therefore, it is necessary to assess the potential of larger HHPs and their oxidation

127 products to substantial SOA formation under different NO_x conditions.

128   In this article, we mainly investigate the detailed mechanisms and kinetic

129 properties of distinct HHPs oxidation initiated by OH radical by employing quantum

130 chemical and kinetics modeling methods. For the resulting H-abstraction products

131 RO_2 radicals, the subsequent reactions involving self-reaction, isomerization and

132 reaction with HO_2 radical are taken into account in the absence of NO, while the

133 subsequent reactions including addition, decomposition and H-abstraction by O_2 are

134 considered in the presence of NO. The investigated HHPs in this work are generated

135 from the bimolecular reactions of distinct carbonyl oxides (CH_2OO, $anti$-CH_3CHOO

136 and $(CH_3)_2COO$) with water vapor.

2. Computational details

2.1 Electronic structure and energy calculations

139   The equilibrium geometries of all the open-shell species, including reactants (R),

140 pre-reactive complex (RC), transition state (TS), post-reactive complex (PC), and

141 products (P), are fully optimized at the unrestricted M06-2X/6-311+G(2df,2p) level of

142 theory (UM06-2X) (Zhao and Truhlar, 2006; Zheng and Truhlar, 2009), whereas all

143 the closed-shell species are optimized at the restricted M06-2X/6-311+G(2df,2p) level

144 of theory (RM06-2X). This is because the M06-2X functional has been proven to

145 produce reliable performance for describing thermochemistry, kinetics and

146 non-covalent interactions (Zhao and Truhlar, 2008). Harmonic vibrational frequencies

147 are performed at the same level to verify that each stationary point is either a true

148 minima (with no imaginary frequency) or a transition state (with one imaginary

149 frequency). Zero-point vibrational energy (ZPVE) and Gibbs free energies corrections

150 (G_{corr}) from harmonic vibrational frequencies are scaled by a factor of 0.98 (Zhao and

151 Truhlar, 2006). The intrinsic reaction coordinate (IRC) calculations are performed to

152 verify the connection between the transition state and the designated reactant and

153 product (Fukui, 1981). The single-point energies are calculated at the

154 (U/R)M06-2X/ma-TZVP level of theory (Zheng, et al., 2011).

155   The tetroxide intermediate formed from the self-reaction of RO_2 radical proceeds

156 through the asymmetric two step O-O bond scission to produce a caged tetroxide

157 intermediate of overall singlet multiplicity comprising two same-spin alkoxyl radicals

158 (spin down) and triplet oxygen (spin up). This type of reaction mechanism can be

159 described by the broken symmetry unrestricted DFT (UDFT) and multi-reference

160 CASSCF methods (Lee et al., 2016; Bach et al., 2005). Previous studies have

161 demonstrated that the UDFT method is suitable to identify the metastable singlet

162 caged radical complex minimum and is successfully located the transition states of

163 O-O bond homolysis, and the energies are comparable to the more accurate and

164 expensive CASSCF method (Lee et al., 2016; Bach et al., 2005). In the present study,

165 the UDFT method is selected to study the asymmetric O-O bond scission and

166 represents a compromise between the computational accuracy and efficiency. The

167 broken symmetry UM06-2X/6-311+G(2df,2p) method is applied to generate the

168 initial guesses of the tetroxide intermediate and transition state geometries with mixed

169 HOMO and LUMO ($S^2 \approx 1$) by using the guess = mix keyword. The single-point

170 energies are refined at the UM06-2X/ma-TZVP level of theory.

171   In order to further evaluate the reliability of the employed method in predicting

172 reaction mechanism, the single-point energies for all the stationary points involved in

173 the initiation reactions of OH radical with distinct HHPs are recalculated at the

174 (U/R)CCSD(T)/6-311+G(2df,2p) level of theory based on the (U/R)M06-2X

175   optimized geometries. Furthermore, the basis set superposition error (BSSE) is also

176   performed to evaluate the stability of the pre-reactive complexes by employing the

177   counterpoise method (Boys and Bernardi, 1970). For simplicity, no prefix is adopted

178   throughout this article. Herein, the Gibbs free energy (G) for each species is obtained

179   by combining the single-point energy with the Gibbs correction ($G = G_{corr} + E$). The

180   electronic energy ($\Delta E_a^{\#}$) and free energy ($\Delta G_a^{\#}$) barriers are defined as the difference

181   in energy between transition state and pre-reactive complex ($\Delta E_a^{\#} = E_{TS} - E_{RC}$ and

182    $\Delta G_a^{\#} = G_{TS} - G_{RC}$). The reaction free energy (ΔG) is referred to the difference in

183   energy between product and reactant ($\Delta G = G_P - G_R$). The calculated $\Delta E_a^{\#}$ and $\Delta G_a^{\#}$

184   for the initiation H-abstraction pathways are summarized in Table S1. As shown in

185   Table S1, the mean absolute deviations (MADs) of $\Delta E_a^{\#}$ and $\Delta G_a^{\#}$ between

186   CCSD(T)/6-311+G(2df,2p) and M06-2X/ma-TZVP approaches are 0.43 and 0.45

187   kcal·mol^{-1}, respectively; the largest deviations of $\Delta E_a^{\#}$ and $\Delta G_a^{\#}$ are 1.2 and 1.1

188   kcal·mol^{-1}, respectively. These results reveal that the energies obtained from the

189   M06-2X/ma-TZVP method are in very good accord with those from the gold-standard

190   coupled-cluster approach CCSD(T) within the uncertainties of systematic errors.

191   Therefore, the M06-2X/ma-TZVP method is selected to investigate the atmospheric

192   degradation of HHP initiated by OH radical under different conditions. In the

193   following sections, unless otherwise stated, the $\Delta G_a^{\#}$ is applied to construct the

194   reaction profiles.

195   For the H-shift reactions of peroxy radicals RO_2, reactants, transition states and

196   products have multiple conformers. Previous literatures have demonstrated that the

197   reaction kinetics of multiconformers involvement are more precisely than that of the

198   single conformer approximation (Møller et al., 2016, 2020). Herein, the

199   multiconformers treatment is performed to investigate the H-shift reactions RO_2

200   radicals. A conformer search within the Molclus program is employed to generate a

201   pool of conformers for RO_2 radicals (Lu, 2020). The selected conformers are further

202   optimized at the M06-2X/6-311+G(2df,2p) level of theory, followed by single-point

203   energies calculations at the M06-2X/ma-TZVP level of theory. On the basis of the

204   calculated Gibbs free energies, the Boltzmann populations (w_i) of each

205    $RO_2 \cdot$ conformer is expressed as eqn 1.

206
$$w_i = \frac{e^{-\Delta G_i / k_B T}}{\sum_i e^{-\Delta G_i / k_B T}}$$
(1)

207   where ΔG_i is the relative Gibbs free energy of conformer i, k_B is the Boltzmann's

208   constant, T is temperature in Kelvin. All the quantum chemical calculations are

209   performed by using the Gaussian 09 program package (Frisch et al., 2009).

2.2 Kinetics calculations

211   The rate coefficients of unimolecular reactions are calculated by using the

212   Rice-Ramsperger-Kassel-Marcus theory coupled with energy-grained master equation

213   (RRKM-ME) method (Holbrook et al., 1996), and the rate coefficients of bimolecular

214   reactions are determined by utilizing traditional transition state theory (TST)

215   (Fernández-Ramos et al., 2007). The RRKM-ME calculations are performed by

216   implementing the MESMER 6.0 program suite (Glowacki et al., 2012). N_2 is used as

217   the buffer gas. The single exponential down model is employed to simulate the

218   collision energy transfer ($<\Delta E>_{down}$ = 200 cm^{-1}). The collisional Lennard-Jones

219   parameters are estimated by using an empirical formula described by Gilbert and

220   Smith (1990). For the H-shift reactions of RO_2 radicals, the rate coefficients are

221   determined by employing the multiconformer transition state theory (MC-TST)

222   approach (Møller et al., 2016). The MC-TST rate coefficient $k_{MC\text{-}TST}$ is calculated by

223   the sum of the individual intrinsic reaction coordinate TST (IRC-TST) rate coefficient

224    $k_{IRC\text{-}TST}$, each weighted by Boltzmann population of corresponding $RO_2 \cdot$ conformer

225   (Møller et al., 2016).

226
$$k_{MC\text{-}TST} = \sum_i^{\text{all TS conf.}} w_i \times k_{IRC\text{-}TST i}$$
(2)

227   where $k_{IRC\text{-}TST i}$ represents the rate coefficient of conformer i, and w_i is the relative

228   Boltzmann population of the corresponding reactant connected to TS$_i$. The

229   one-dimensional asymmetry Eckart model is employed to calculate the tunneling

230   correction (Eckart, 1930). Considering the uncertainty in barrier heights ($\sim$ 1.0

231   kcal mol^{-1} by the M06-2X method) and in tunneling corrections, the uncertainty of the

232 calculated rate coefficient is about one order of magnitude in the present study.

3. Results and discussion

3.1 Initiation reaction of HHPs with OH radical

235   Previous literatures have proposed that the lifetime of CI with respect to the
236 reaction with water vapour exhibits a highly dependent on the nature of CIs (Anglada
237 and Solé, 2016; Taatjes et al., 2013; Anglada et al., 2011), and the primary product is
238 HHPs in both gas phase and air/water interface (Chao et al., 2015; Chen et al., 2016a;
239 Smith et al., 2015; Zhu et al., 2016; Zhong et al., 2018). In the present study, we
240 mainly consider three kinds of HHPs originated from the addition of water to CH_2OO
241 and methyl-substituted CI (*anti*-CH_3CHOO and $(CH_3)_2COO$). The lowest-energy
242 conformers HHP ($HOCH_2OOH$, $HOCH(CH_3)OOH$ and $HOC(CH_3)_2OOH$) are
243 obtained from the previous study as shown in Figure 1 (Chen et al., 2019), and they
244 are selected as model system to investigate the atmospheric degradation mechanism
245 of HHP initiated by OH radical. Letters and numbers are applied to mark carbon,
246 oxygen and hydrogen atoms in different reaction sites.
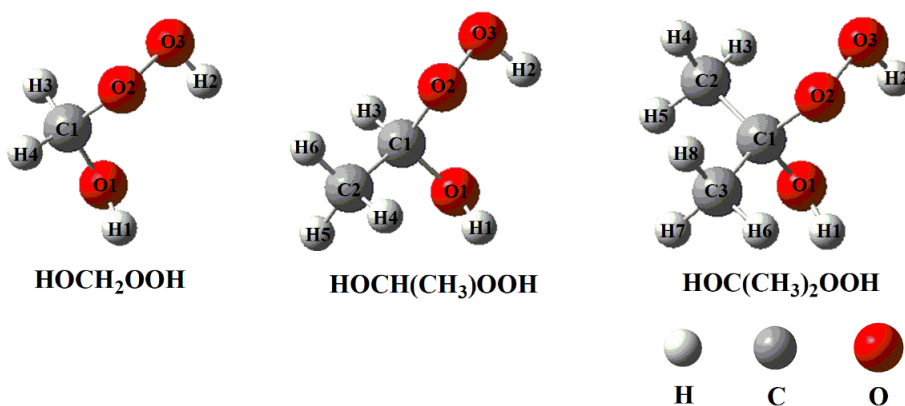
247
248   **Figure 1.** The structures of distinct HHPs

249   The free-energy and electronic-energy potential energy surfaces (PESs) for the
250 initiation reactions of OH radical with $HOCH_2OOH$, $HOCH(CH_3)OOH$ and
251 $HOC(CH_3)_2OOH$ are presented in Figures 2-4 and S1-S3, respectively. And the
252 optimized geometries of all the stationary points are displayed in Figures S6-S8,
253 respectively. As can be seen in Figure 2, the reaction for $HOCH_2OOH$ with OH
254 radical proceeds via four distinct pathways: H-abstraction from the -O_1H_1 (R1), -C_1H_3

255   (R2), -C_1H_4 (R3) and -$O_2O_3H_2$ groups (R4). For each pathway, a pre-reactive complex

256   with a six- or seven-membered ring structure is formed in the entrance channel, which

257   is stabilized by hydrogen bond interactions between the oxygen atom of OH radical

258   and the abstraction hydrogen atom of $HOCH_2OOH$, and the remnant hydrogen atom

259   of OH radical and one of oxygen atoms of $HOCH_2OOH$ (Figure S6). Then, it

260   surmounts modest barrier that is higher in energy than the reactants to reaction. The

261   reaction barrier $\Delta G_a^{\#}$ are reduced in the order of 6.4 (R1) > 5.8 (R2) $\approx$ 5.4 (R3) > 1.5

262   (R4) kcal mol^{-1}, indicating that H-abstraction from the -$O_2O_3H_2$ group (R4) is more

263   preferable than those from the -O_1H_1, -C_1H_3 and -C_1H_4 groups (R1-R3). Same

264   conclusion is also derived from the energy barriers $\Delta E_a^{\#}$ that R4 is the most favorable

265   H-abstraction pathway (Figure S1). The difference of barrier heights can be attributed

266   to the bond dissociation energy (BDE) of different types of bonds in $HOCH_2OOH$

267   molecule. The BDE are decreased in the order of 103.7 (O_1-H_1) > 98.2 (C_1-H_3) $\approx$ 97.4

268   (C_1-H_4) > 87.2 (O_3-H_2) kcal mol^{-1}, which are in good agreement with the order of

269   barrier heights of H-abstraction reactions. As indicated by their reaction free energy

270   values, it can be found that the exothermicity of R4 is the largest among these four

271   H-abstraction reactions. Based on the above discussions, it is concluded that

272   H-abstraction from the -$O_2O_3H_2$ group resulting in formation of $HOCH_2OO$ radical

273   (R4) is feasible on both thermodynamically and kinetically.

274   Considering the different reaction sites of hydrogen atoms, the atmospheric

275   transformation of $HOCH(CH_3)OOH$ from the *anti*-CH_3CHOO + H_2O reaction should

276   have six types of H-abstraction pathways as presented in Figure 3. As shown in Figure

277   3, each H-abstraction reaction begins with the formation of a weakly bound hydrogen

278   bonded pre-reactive complex with a six- or seven-membered ring structure in the

279   entrance channel (Figure S7). Then it immediately transforms into the respective

280   product via the corresponding transition state. The $\Delta G_a^{\#}$ of H-abstraction from the

281   -C_1H_3 (R6) and -$O_2O_3H_2$ (R8) groups are 2.2 and 1.7 kcal mol^{-1}, respectively, which

282   are ~ 4-5 kcal mol^{-1} lower than those from the -O_1H_1 (R5) and -CH_3 groups (R7). This

283   result shows that R6 and R8 have nearly identical importance in the atmosphere.

284   Compared with the barriers of H-abstraction at the C_α (R6) and C_β (R7) positions, it

285   can be found that the former case is more favourable than the latter case. This

286   conclusion is further supported by Jara-Toro's study for the reactions of OH radical

287   with linear saturated alcohols (methanol, ethanol and n-propanol) that H-abstraction at

288   the C_α position is predominant (Jara-Toro, R. A et al., 2017, 2018).

289   For the OH-initiated oxidation of $HOCH(CH_3)OOH$ from the *syn*-CH_3CHOO +

290   H_2O reaction, the corresponding free-energy and electronic-energy PESs are

291   displayed in Figures S4 and S5, respectively. From Figure S4, it can be seen the

292   H-abstraction by OH radical from $HOCH(CH_3)OOH$ has six kinds of pathways. For

293   each pathway, a per-reactive complex is formed prior to the corresponding transition

294   state, and then it overcomes modest barrier to reaction. The $\Delta G_a^{\#}$ of R6' and R8' are

295   2.3 and 1.8 kcal·mol^{-1}, respectively, which are about 5 kcal·mol^{-1} lower than those of

296   R5' and R7'. This result shows that H-abstraction from the -CH (R6') and -OOH (R8')

297   groups are preferable kinetically. Same conclusion is also derived from the energy

298   barriers $\Delta E_a^{\#}$ that the R6' and R8' the most favourable H-abstraction pathways (Figure

299   S5). It should be noted that although the barriers of R6' and R8' are comparable, the

300   exoergicity of the former case is significantly lower than that of the latter case. The

301   above-mentioned conclusions are consistent with the results derived from the

302   OH-initiated oxidation of $HOCH(CH_3)OOH$ from the *anti*-CH_3CHOO + H_2O reaction.

303   Zhou et al. has demonstrated that the bimolecular reaction of *syn*-CH_3CHOO with

304   water leading to the formation of $HOCH(CH_3)OOH$ is of less importance in the

305   atmosphere, while the unimolecular decay to OH radical is the major loss process of

306   *syn*-CH_3CHOO (Zhou et al., 2019). Therefore, in the present study, we mainly focus

307   on the subsequent mechanism of intermediate generated from OH-initiated oxidation

308   of $HOCH(CH_3)OOH$ from the *anti*-CH_3CHOO + H_2O reaction.

309   From Figure 4, it can be seen that H-abstraction from $HOC(CH_3)_2OOH$

310   includes eight possible H-abstraction pathways. All the H-abstraction reactions are

311   strongly exothermic and spontaneous, signifying that they are thermodynamically

312   feasible under atmospheric conditions. It deserves mentioning that the release of

313   energy of R12 is significantly greater than those of R9-R11. For each H-abstraction

314   pathway, a RC with a six- or seven-membered ring structure is formed prior to the

corresponding TS, which is more stable than the separate reactants due to the hydrogen bond interactions between $HOC(CH_3)_2OOH$ and OH radical. Then, the RC overcomes modest barrier to reaction. The $\Delta G_a^{\#}$ of H-abstraction from the $-O_2O_3H_2$ group (R12) is 2.7 kcal mol^{-1}, which is the lowest among these eight H-abstraction reactions. This result again shows that the H-abstraction from the $-O_2O_3H_2$ group is the dominant pathway.

The rate coefficients of every H-abstraction pathway involved in the initiation reactions of distinct HHPs with OH radical are estimated over the temperature range from 273 to 400 K as summarized in Table S2-S4 and Figures S9-S11. As shown in Table S2, the total rate coefficients k_{tot} of $HOCH_2OOH$ reaction with OH radical are slightly decreased with the temperature increasing. At ambient temperature, k_{tot} is estimated to be 3.3×10^{-11} cm^3 molecule^{-1} s^{-1}, which is a factor of ~5 greater than the Allen's result $((7.1 \pm 1.5) \times 10^{-12}$ cm^3 molecule^{-1} s^{-1}, at 295 K) derived from the reaction of HMHP with OH radical by using the CF_3O^- chemical ionization mass spectrometry (CIMS) and laser-induced fluorescence (LIF) (Allen et al., 2018). Such a discrepancy could be attributed to the uncertainty in barrier height and tunneling correction. $k_{R4(O3-H2)}$ is 1-2 orders of magnitude greater than $k_{R1(O1-H1)}$, $k_{R2(C1-H3)}$ and $k_{R3(C1-H4)}$ in the whole temperature range, implying that R4 is the most favorable H-abstraction pathway. For example, $k_{R4(O3-H2)}$ is calculated to be 2.9×10^{-11} cm^3 molecule^{-1} s^{-1} at 298 K, which is higher than $k_{R1(O1-H1)}$ (1.8×10^{-13}), $k_{R2(C1-H3)}$ (9.9×10^{-13}) and $k_{R3(C1-H4)}$ (2.0×10^{-12}) by 161, 29 and 15 times, respectively.

From Table S3, it can be seen that the total rate coefficients k'_{tot} of $HOCH(CH_3)OOH$ reaction with OH radical are decreased in the range of 4.5×10^{-11} (273 K) to 8.1×10^{-12} (400 K) cm^3 molecule^{-1} s^{-1} with increasing temperature, and they exhibit a slightly negative temperature dependence. $k_{R8(O3-H2)}$ are approximately identical to k'_{tot} in the entire temperature range, which are 1-2 orders of magnitude greater than $k_{R5(O1-H1)}$, $k_{R6(C1-H3)}$, $k_{R7-1(C2-H4)}$, $k_{R7-2(C2-H5)}$ and $k_{R7-3(C2-H6)}$. The result again shows that H-abstraction from the -OOH group (R8) is preferable kinetically. It should be noted that although the barriers of R8 and R6 are comparable, $k_{R8(O3-H2)}$ is about one order of magnitude higher than $k_{R6(C1-H3)}$ over the temperature range studied.

345 The reason is most likely due to the stability of pre-reactive complexes that IM8-a is

346 more stable than IM6-a in energy. A similar conclusion is derived from the results of

347 rate coefficient of $HOC(CH_3)_2OOH + OH$ reaction that H-abstraction from the -OOH

348 group (R12) is favorable kinetically (Table S4). The concentrations of OH radical

349 vary from 5 to 15 $\times 10^6$ molecules cm^{-3} during daylight (Long et al., 2017), resulting

350 in the atmospheric lifetime of $HOCH_2OOH$, $HOCH(CH_3)OOH$ and $HOC(CH_3)_2OOH$

351 reactivity toward OH radical are estimated to be 0.58-1.74 h, 0.60-1.79 h and

352 1.23-3.69 h at room temperature.

353   In summary, the dominant pathway is the H-abstraction from the -OOH group in

354 the initiation reactions of OH radical with $HOCH_2OOH$. H-abstraction from -CH

355 group is competitive with that from the -OOH group in the reaction of OH radical

356 with $HOCH(CH_3)OOH$. Compared the barriers of H-abstraction from the -OOH and

357 -CH_2 groups in the OH + $HOCH_2OOH$ system with that for the analogous reactions

358 in the OH + $HOCH(CH_3)OOH$ system. It can be found that the barrier of

359 H-abstraction from the -CH group is reduced by 3.6 kcal mol^{-1}, whereas the barrier

360 of H-abstraction from the -OOH group is increased by 0.2 kcal mol^{-1} when a methyl

361 group substitution occurs at the C1-position of $HOCH_2OOH$. The dominant pathway

362 is the H-abstraction from the -OOH group in the reaction of OH radical with

363 $HOC(CH_3)_2OOH$, and the barrier height is increased by 1.2 kcal mol^{-1} compared to

364 the OH + $HOCH_2OOH$ system. The barrier of H-abstraction from the -OOH group

365 is slightly increased as the number of methyl group is increased. It is interesting to

366 compare the rate coefficient of dominant pathway in the OH + $HOCH_2OOH$ system

367 with that for the analogous reactions in the OH + $HOCH(CH_3)OOH$ and OH +

368 $HOC(CH_3)_2OOH$ reactions. It can be found that the rate coefficient is almost

369 identical when a methyl group substitution occurs at the C_1-position, whereas the

370 rate coefficient reduces by a factor of 2-5 when two methyl groups introduce into the

371 C_1-position.

372
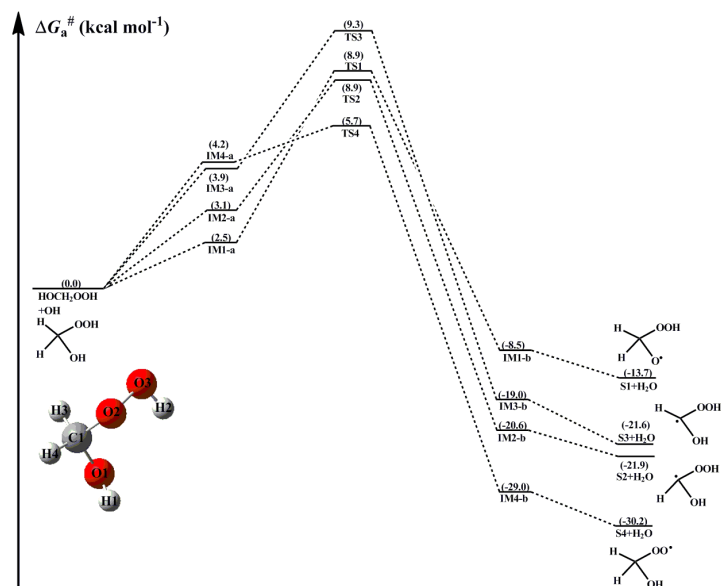
Figure 2. PES ($\Delta G_a^{\#}$) for the OH-initiated reactions of $HOCH_2OOH$ from the $CH_2OO + H_2O$ reaction predicted at the M06-2X/ma-TZVP//M06-2X/6-311+G(2df,2p) level of theory (a and b represent the pre-reactive and post-reactive complexes)

376
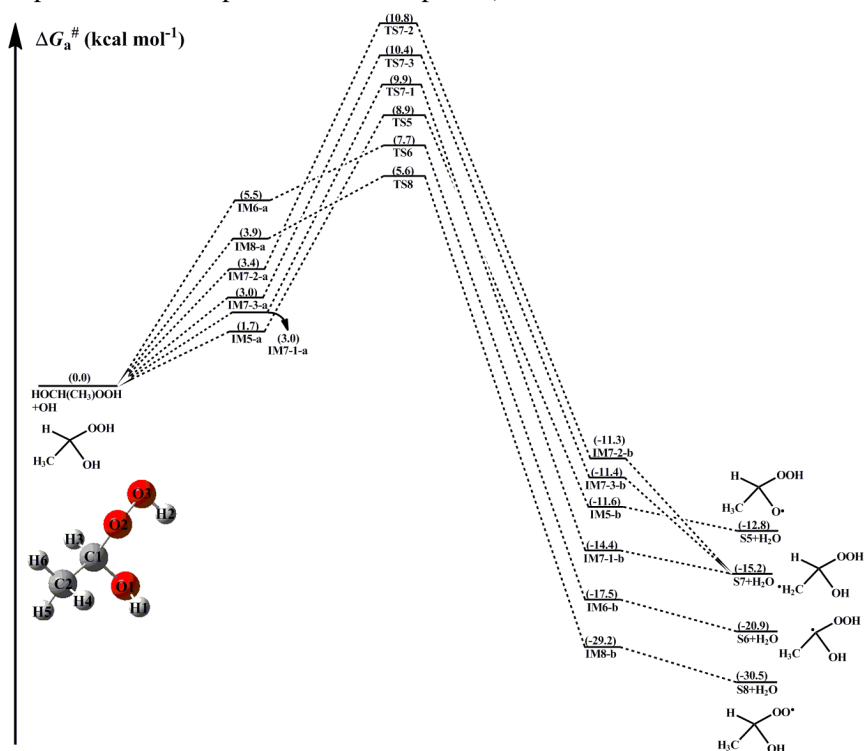
Figure 3. PES ($\Delta G_a^{\#}$) for the OH-initiated reactions of $HOCH(CH_3)OOH$ from the *anti*-$CH_3CHOO + H_2O$ reaction predicted at the M06-2X/ma-TZVP//M06-2X/6-311+G(2df,2p) level of theory (a and b represent the pre-reactive and post-reactive complexes)
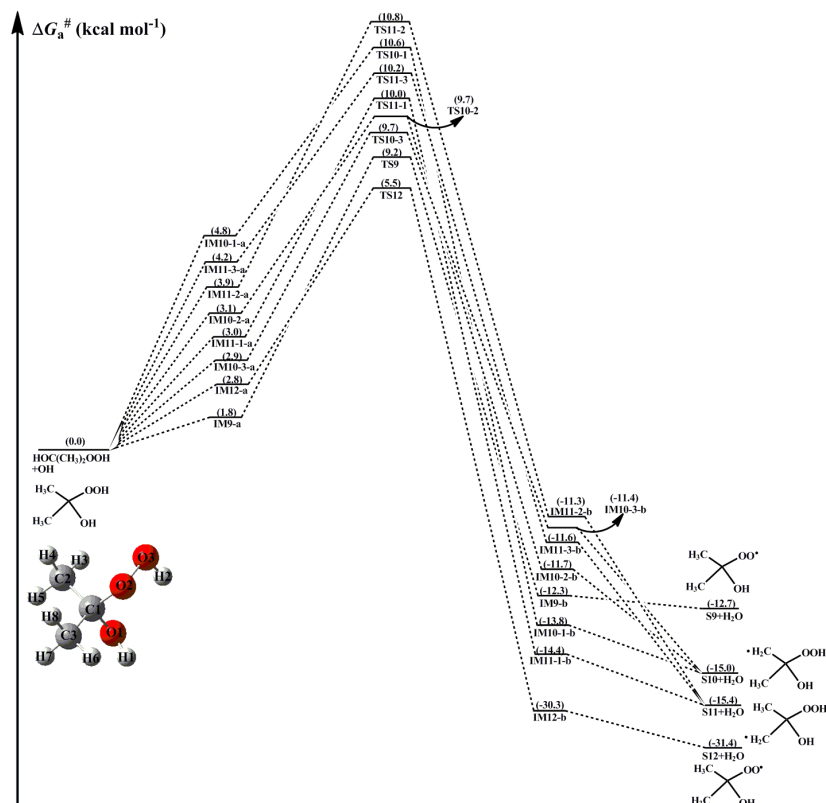
Figure 4. PES ($\Delta G_a^{\#}$) for the OH-initiated reactions of HOC(CH$_3$)$_2$OOH from the (CH$_3$)$_2$COO + H$_2$O reaction predicted at the M06-2X/ma-TZVP//M06-2X/6-311+G(2df,2p) level of theory (a and b represent the pre-reactive and post-reactive complexes)

3.2 Subsequent reactions of H-abstraction products RO$_2$ radicals in pristine environment

In principle, the H-abstraction products RO$_2$ radicals have three types of channels in pristine environment: (1) the self-reactions of RO$_2$ radicals can either produce RO · + R'O · + O$_2$ (propagation channel), or generate ROH + R'(-H, =O) + O$_2$ or produce ROOR + O$_2$ (termination channel) that has been recognized as an important SOA precursor (Berndt et al., 2018; Zhang et al., 2012); (2) RO$_2$ radicals react with HO$_2$ radical leading to the formation of hydroperoxide ROOH, alcohol, OH and other products (Winiberg et al., 2016; Chen et al., 2021); (3) RO$_2$ radicals autoxidation through intramolecular H-shift and alternating O$_2$ addition steps generate HOMs (Ehn et al., 2014; Bianchi et al., 2019; Nozière and Vereecken, 2019; Rissanen et al., 2014). The relevant details for these three kinds of reactions will be discussed in the following paragraph.

3.2.1 Reactions mechanism for the self-reaction of RO_2 radicals

The self-reaction is one of dominant removal pathways for RO_2 radicals when the concentration of NO is low. The self-reaction of RO_2 radicals usually follows the Russell mechanism (Russell, 1957), and mainly includes four kinds of pathways: (1) $2RO_2 \cdot \rightarrow 2RO \cdot + O_2$; (2) $2RO_2 \cdot \rightarrow ROH + RCO + O_2$; (3) $2RO_2 \cdot \rightarrow ROOR + O_2$; (4) $2RO_2 \cdot \rightarrow ROOH + R'CHOO$ (Atkinson and Arey, 2003). The relative importance of different pathways varies considerably depending on the nature of RO_2 radicals (Valiev et al., 2019; Lee et al., 2016). A schematic PES for the self-reaction of $HOCH_2OO$ radical is drawn in Figure 5. As can be seen in Figure 5a, the self-reaction of $HOCH_2OO$ radical starts with the formations of tetroxide complexes IM13-a and IM14-a in the entrance channel, with 2.9 and 3.4 kcal mol^{-1} stability. Then they fragment into dimer S13 + $^1O_2$ (R13) and $HOCH_2OOH$ + HOCHOO (R14) via transition states TS13 and TS14 with the barriers of 43.3 and 51.5 kcal mol^{-1}. But the barriers of R13 and R14 are extremely high, making them irrelevant in the atmosphere.

From Figure 5b, it is seen that the self-reaction of $HOCH_2OO$ radical proceeds via oxygen-to-oxygen coupling leading to the formation of tetroxide intermediate S14 with the electronic energy and free energy barriers of 7.3 and 19.6 kcal mol^{-1}. Kumar and Francisco reported that the electronic energy barrier of the gas phase decomposition of $HOCH_2OO$ radical is 14.0 kcal mol^{-1} and it could be a new source of HO_2 radical in the troposphere (Kumar and Francisco, 2015, 2016). Compared with the electronic energy barriers of unimolecular dissociation of $HOCH_2OO$ radical and its self-reaction, it can be found that the self-reaction of $HOCH_2OO$ radical resulting in formation of S14 is significantly feasible. The formed S14 can fragment into $HOCH_2O \cdot$ + HCOOH + $HO_2 \cdot$ via a concerted process of O_2-O_3 and O_5-O_6 bonds rupture and O_3-H_6 bond forming with the barrier of 29.8 kcal mol^{-1}. Alternatively, S14 can convert into the caged tetroxide intermediate S16 through the asymmetric two step O_2-O_3 and O_5-O_6 bonds scission with the barriers of 19.1 and 3.1 kcal mol^{-1}, respectively. The result shows that the latter pathway is more preferable than the

former channel owing to its lower barrier. The overall spin multiplicity of S16 is singlet, in which the O_2 moiety maintains the triplet ground state (spin up) and is very loosely bound. In order to preserve the overall singlet multiplicity, the two $HOCH_2O$ radical pairs ($^3(HOCH_2O \cdots HOCH_2O)$) must have the triplet multiplicity (spin down). S16 could be regarded as the ground state $^3O_2$ moving away from the two $HOCH_2O$ radical pairs that keep interacting. Due to the difficulty in performing the constrained optimization for the dissociation of S16, the $^3O_2$ moiety is considered as a leaving moiety away from two $HOCH_2O$ radical pairs, and merely the dissociation of $^3(HOCH_2O \cdots HOCH_2O)$ is taken into consideration in the present study. It has three types of pathways: (1) it yields $HOCH_2OH$ and excited-state ^3HCOOH through the alpha hydrogen transfer with the barrier of 14.0 kcal mol^{-1} and 10.2 kcal mol^{-1} exothermicity, followed by the excited ^3HCOOH to go back to the ground-state ^1HCOOH; (2) it generates two $HOCH_2O$ radicals via the barrierless process with the exoergicity of 16.9 kcal mol^{-1}; (3) it produces dimer S17 via an intersystem crossing (ISC) step with the exoergicity of 32.1 kcal mol^{-1}. Based on the calculated reaction barriers, it can be found that the rate-limiting step is the cleavage of O_2-O_3 bond (R17) in the unimolecular decay processes of S14. This conclusion coincides with the previous result obtained from the dissociation of di-t-butyl tetroxide that the rate-controlling step is the rupture of single O-O bond (Lee et al., 2016). Valiev et al. proposed that the ISC rate of ROOR dimer formed from the different (RO $\cdots$ R'O) systems is extremely rapid ($> 10^8$ s^{-1}) and exhibits a strong stereoselectivity (Valiev et al., 2019).

Figure 6 depicts a schematic PES for the self-reaction of $HOCH(CH_3)OO$ radical. As shown in Figure 6a, the self-reaction of $HOCH(CH_3)OO$ radical can either produce dimer S18 along with $^1O_2$ via transition state TS20 with the barrier of 44.4 kcal mol^{-1}, or generate $HOCH(CH_3)OOH$ and $HOC(CH_3)OO$ though transition state TS21 with the barrier of 54.3 kcal mol^{-1}. But the barriers of R20 and R21 are significantly high, making them are of less importance in the atmosphere. Alternatively, the self-reaction of $HOCH(CH_3)OO$ radical proceeds via an oxygen-to-oxygen coupling resulting in formation of tetroxide intermediate S19 with

456   the barrier of 19.9 kcal mol^{-1} (Figure 6b). The formed S19 proceeds through the

457   asymmetric two step O_2-O_3 and O_5-O_6 bonds scission to produce a caged tetroxide

458   intermediate S21 of overall singlet multiplicity comprising two same-spin alkoxyl

459   radicals (spin down) and triplet oxygen (spin up). These two processes accompany

460   with the barriers of 21.4 and 1.3 kcal mol^{-1}, respectively. Then it decomposes into the

461   propagation (2HOCH(CH$_3$)O · + ^{3}O$_2$) and termination products (HOCH(CH$_3$)OH +

462   ^{3}CH$_3$OOH + ^{3}O$_2$ and dimer S22 + ^{3}O$_2$) with the exoergicity of 12.5, 11.7 and 33.0

463   kcal mol^{-1}. The rate-determining step is the rupture of O_2-O_3 bond (R24) in the

464   dissociation processes of S19.

465   As shown in Figure 7, the dominant pathway for the self-reaction of

466   HO(CH$_3$)$_2$COO radical begins with the formation of tetroxide intermediate S24 via an

467   oxygen-to-oxygen coupling transition state TS28 with the barrier of 20.4 kcal mol^{-1};

468   then it transforms into the caged tetroxide intermediate S26 of overall singlet spin

469   multiplicity through the asymmetric two-step O-O bond cleavage with the barriers of

470   22.0 and 3.4 kcal mol^{-1}; finally, S26 can either produce two HO(CH$_3$)$_2$CO radicals

471   with the exoergicity of 10.3 kcal mol^{-1}, or generate dimer S27 with the exothermicity

472   of 31.5 kcal mol^{-1}. Different the self-reactions of HOCH$_2$OO and HOCH(CH$_3$)OO

473   radicals, the termination product of the self-reaction of HOC(CH$_3$)$_2$OO radical is

474   exclusively dimer S27. The reason is due to the absence of alpha hydrogen atom in

475   HOC(CH$_3$)$_2$OO radical. Compared with the barrier of rate-determining route R17 in

476   the self-reaction of HOCH$_2$OO radical, it can be found that the barrier of rate-limiting

477   step R29 is increased by about 3.0 kcal mol^{-1} when two methyl substitutions introduce

478   into the C1-position of HOCH$_2$OO radical. The reason might be attributed to the cage

479   escape of alkoxyl radicals. It is therefore that the tertiary RO$_2$ radicals have great

480   opportunity to react with HO$_2$ radical or autoxidation in pristine environment.

481

482
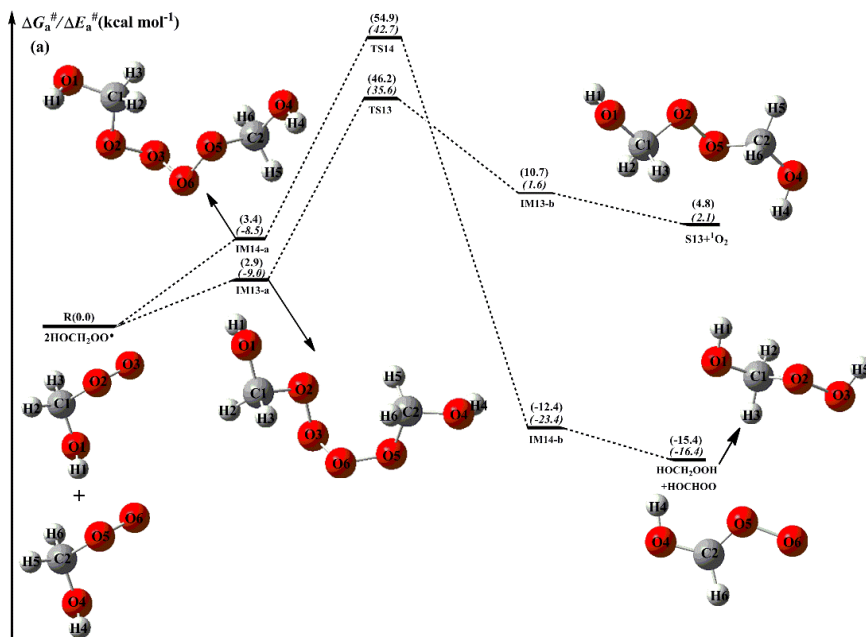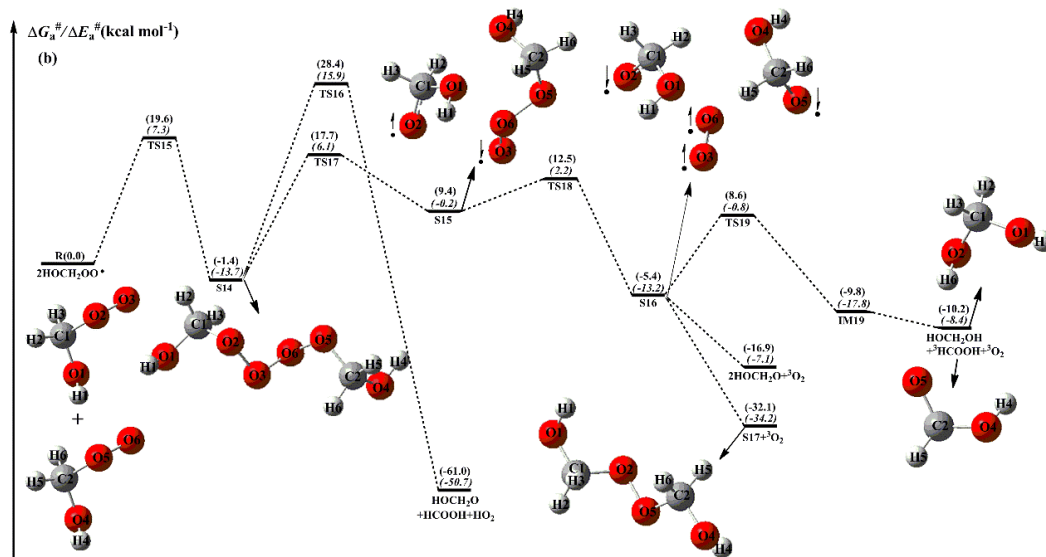
Figure 5. PES ($\Delta G_a^{\#}$ and $\Delta E_a^{\#}$, in italics) for the self-reaction of $HOCH_2OO$ radicals predicted at
the M06-2X/ma-TZVP//M06-2X/6-311+G(2df,2p) level of theory

485

486
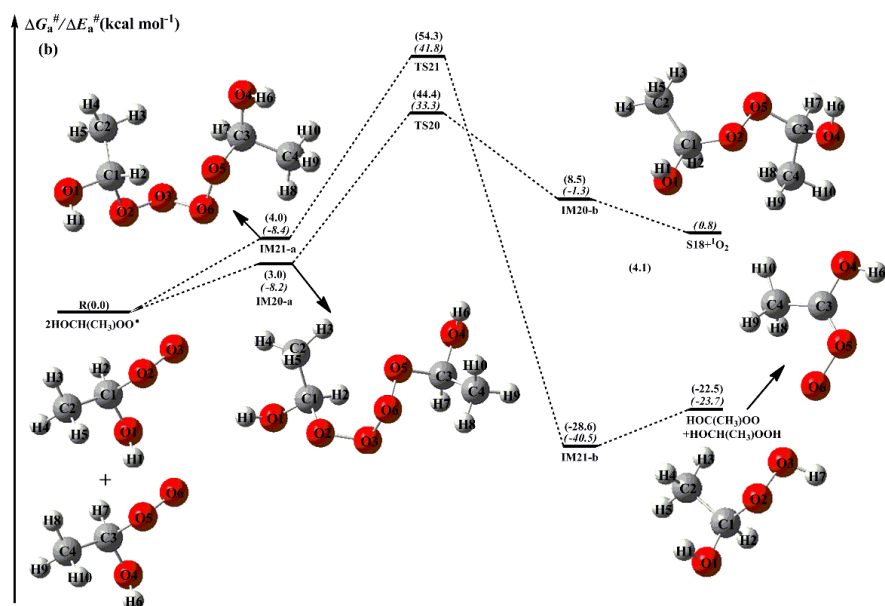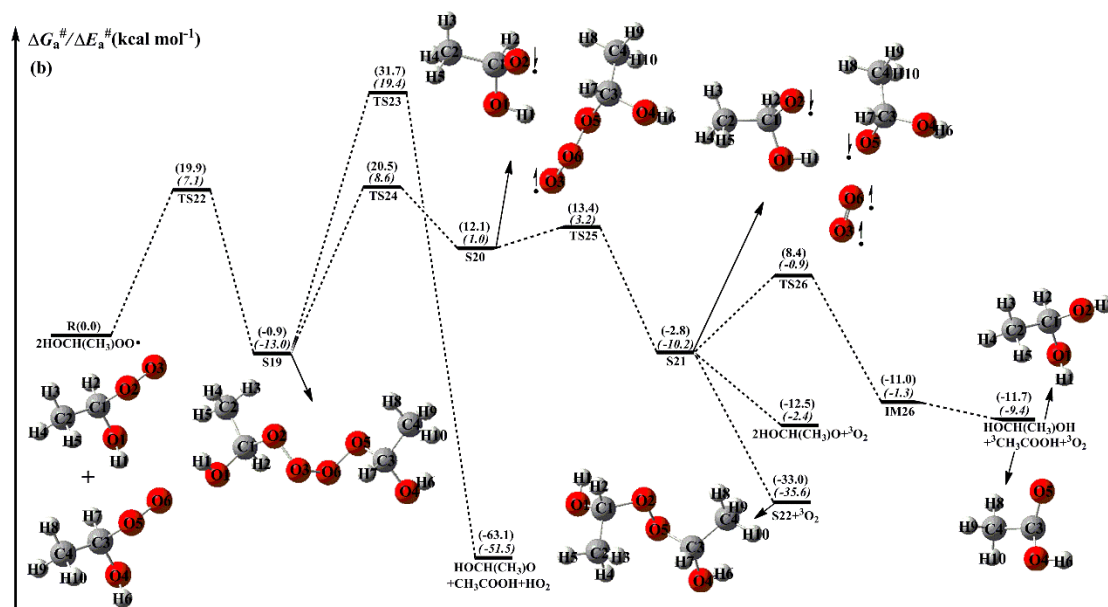
Figure 6. PES ($\Delta G_a^{\#}$ and $\Delta E_a^{\#}$, in italics) for the self-reaction of HOCH(CH$_3$)OO radicals predicted at the M06-2X/ma-TZVP//M06-2X/6-311+G(2df,2p) level of theory
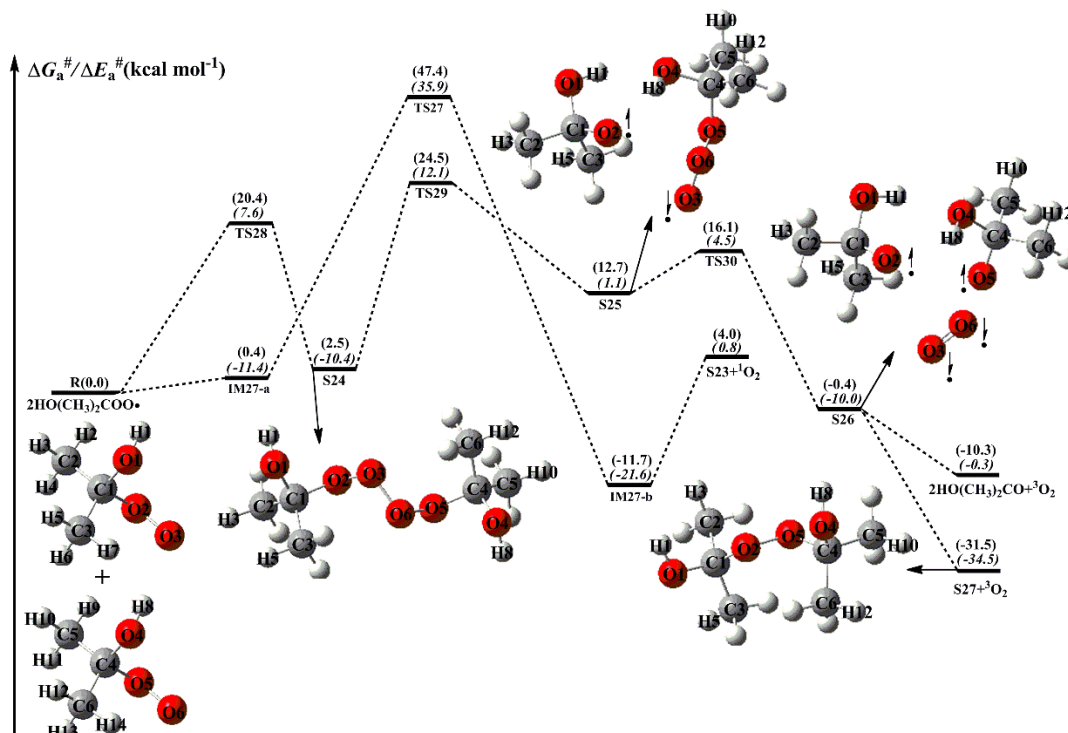
Figure 7. PES ($\Delta G_a^{\#}$ and $\Delta E_a^{\#}$, in italics) for the self-reaction of $HO(CH_3)_2COO$ radicals predicted at the M06-2X/ma-TZVP//M06-2X/6-311+G(2df,2p) level of theory

3.2.2 Reactions mechanism for the reaction of RO_2 radicals with HO_2 radical

When NO is present in low concentration, the bimolecular reaction of RO_2 radicals with HO_2 radical is generally expected to be the dominant pathway as the main product hydroperoxide ROOH. The main sources of HO_2 radical involve the photo-oxidation of oxygenated volatile organic compounds (OVOCs) and the ozonolysis reaction, as well as senondary sources include the reactions of OH radical with CO, ozone and volatile organic compounds (VOCs), the reaction of alkoxy radical RO with O_2 and the red-light-induced decomposition of α-hydroxy methylperoxy radical $OHCH_2OO$ (Kumar et al., 2015; Stone et al., 2012; Hofzumahaus et al., 2009). The atmospheric concentration of HO_2 radical is 1.5-10 $\times$ 10^8 molecules cm^{-3} at ground level in polluted urban environments (Stone et al., 2012). A schematic PES for the reactions of distinct RO_2 radicals with HO_2 radical is presented in Figure 8. As shown in Figure 8, all the reactions are strongly exothermic and spontaneous, indicating that they are feasible thermodynamically in the atmosphere. The reaction for $HOCH_2OO \cdot$ with $HO_2 \cdot$ (R31) starts with the formation

508 of a pre-reactive complex IM31-a in the entrance channel, which is more stable than

509 the separate reactants by 3.8 kcal·mol^{-1} in energy. Then it converts into HOCH$_2$OOH

510 and O$_2$ via a hydrogen atom transfer from the HO$_2$ radical to the terminal oxygen

511 atom of HOCH$_2$OO radical with the barrier of 2.0 kcal·mol^{-1}. The mechanism of

512 HOCH(CH$_3$)OO· + HO$_2$·(R32) and HO(CH$_3$)$_2$COO· + HO$_2$·(R33) reactions is quite

513 similar to that of HOCH$_2$OO· + HO$_2$·system. In order to avoid redundancy, we will

514 not discuss them in detail. It deserves mentioning that the barrier height is only

515 reduced by 0.1 kcal·mol^{-1} when one or two methyl substitutions occur at the

516 C1-position of HOCH$_2$OO radical, compared to the barrier of HOCH$_2$OO· +

517 HO$_2$·reaction. This result implies that the barrier height is not seem to be influenced

518 by the number of methyl substitution. The rate coefficients of distinct RO$_2$ radicals

519 reactions with HO$_2$ radical are summarized in Table S5 and Figure S12. As shown in

520 Table S5, the rate coefficients k_{R31} of HOCH$_2$OO· + HO$_2$ reaction vary from 3.1 ×

521 10^{-11} (273 K) to 2.1 × 10^{-12} cm^3 molecule^{-1} s^{-1} (400 K), and they exhibit a negative

522 temperature dependence. Similar conclusion is also obtained from the rate coefficients

523 k_{R32} and k_{R33} that they are decreased with the temperature increasing. It should be

524 noted that the rate coefficient is slightly increased as the number of methyl group is

525 increased. At ambient temperature, k_{R31} is estimated to be 1.7 × 10^{-11} cm^3 molecule^{-1}

526 s^{-1}, which is in good agreement with the value of ~2 × 10^{-11} cm^3 molecule^{-1} s^{-1} for the

527 reaction of acyl peroxy radicals with HO$_2$ radical (Wennberg et al., 2018). The typical

528 atmospheric concentrations of HO$_2$ radical are about 5, 20 and 50 pptv in the urban,

529 rural and forest environments (Bianchi et al., 2019), translating into the

530 pseudo-first-order rate constants $k'_{HO2} = k_{HO2}$[HO$_2$] of 1.1 × 10^{-3}, 4.2 × 10^{-3} and 1.1 ×

531 10^{-2} s^{-1}, respectively. The pseudo-first-order rate constants of R32 and R33 are

532 predicted to be 3.0 × 10^{-3} and 4.8 × 10^{-3} (urban), 1.1 × 10^{-2} and 1.8 × 10^{-2} (rural), 3.0

533 × 10^{-2} and 4.8 × 10^{-2} s^{-1} (forest) at room temperature.

534
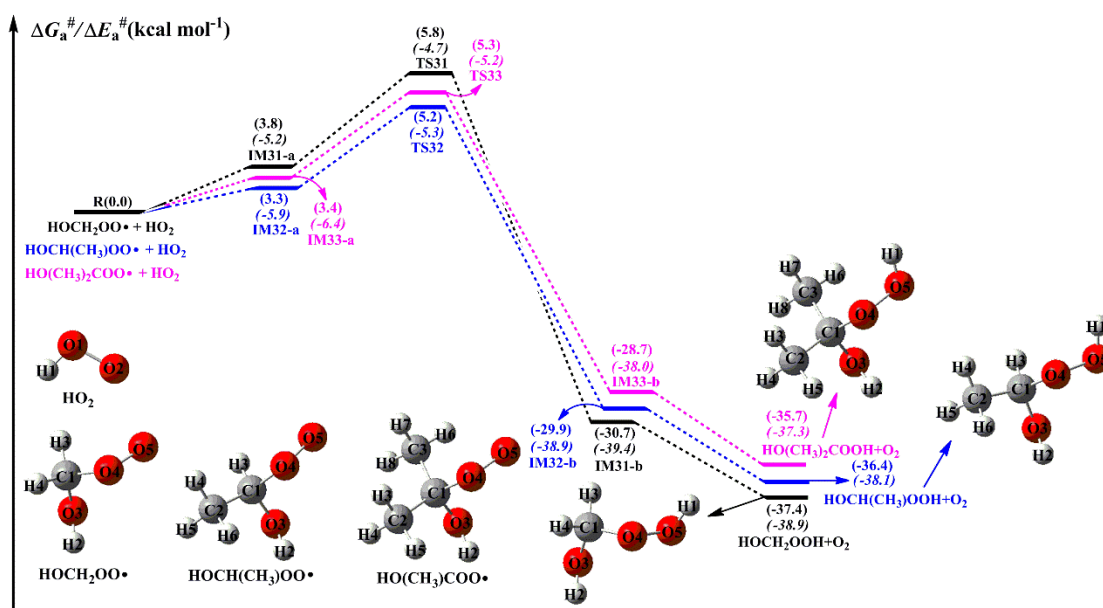
Figure 8. PES ($\Delta G_a^{\#}$ and $\Delta E_a^{\#}$, in italics) for the reactions of HO_2 radical with distinct RO_2 radicals predicted at the M06-2X/ma-TZVP//M06-2X/6-311+G(2df,2p) level of theory

3.2.3 Reactions mechanism for the isomerization of RO_2 radicals

Autoxidation of RO_2 radicals is known to play an important role in the (re)generation of HO_x radicals and in the formation of HOMs (Wang et al., 2017; Bianchi et al., 2019; Rissanen et al., 2014; Ehn et al., 2017). The autoxidation mechanism includes an intramolecular H-shift from the $-CH_3$ or $-CH_2-$ groups to the $-OO \cdot$ site, resulting in formation of a hydroperoxyalkyl radical QOOH, followed by O_2 addition to form a new peroxy radical ($HOOQO_2$), one after the other, and the resulting finally HOMs (Rissanen et al., 2014; Berndt et al., 2015). For the H-shift reactions of RO_2 radical, reactants, transition states and products have multiple conformers due to the effect of degree of freedom for internal rotation. Based on the calculated results, it can be found that $HOCH_2OO$ radical has four energetically similar conformers ($HOCH_2OO$-a, $HOCH_2OO$-b, $HOCH_2OO$-c and $HOCH_2OO$-d). The relative free energy and Boltzmann population (w_i) of individual conformer are listed in Table S6. As shown in Table S6, the Boltzmann populations of these four conformers are 46.39, 46.31, 2.99 and 4.32%, respectively.

A schematic PES for the H-shift reactions of $HOCH_2OO$ radical is displayed in Figure 9. As can be seen in Figure 9, the lowest-energy conformer $HOCH_2OO$-a can proceed via a 1,3-H shift from the $-CH_2$ group to the terminal oxygen leading to the

556   formation of S28-a (HO CHOOH) with the barrier of 41.6 kcal·mol^{-1}. HOCH$_2$OO-b

557   can isomerize to S28-b1 and S28-b2 via the four-membered ring transition states

558   TS34-b1 and TS34-b2 (1,3-H shifts) with the barriers of 41.6 and 45.0 kcal·mol^{-1}. But

559   these three 1,3-H shift reactions have comparatively high barriers, making them

560   irrelevant in the atmosphere. Despite many attempts, the transition states of H-shift

561   reactions of HOCH$_2$OO-c and HOCH$_2$OO-d are not located. The result implies that

562   the H-shift reactions of these two conformers are inhibited, which is consistent with

563   the previous study that not all reactants will be in a conformation with a path across

564   the barrier to reaction in the H-shift reactions of RO$_2$ radicals (Møller et al., 2016).

565   Equivalent to the case of HOCH$_2$OO radical, the isomerization of HOCH(CH$_3$)OO

566   radical proceeds via the 1,3- and 1,4-H shifts from the -CH or -CH$_3$ groups to the

567   terminal oxygen resulting in formation of hydroperoxyalkyl radicals (Figure S13).

568   These 1,3- and 1,4-H shift reactions accompany with the extremely high barriers (>

569   37.9 kcal·mol^{-1}), implying that they are of less importance in the atmosphere. Similar

570   conclusion is also derived from the isomerization of HO(CH$_3$)$_2$COO radical that 1,4-H

571   shift reactions are unfavourable kinetically (Figure S14). The high barriers of 1,3- and

572   1,4-H shifts can be interpreted as the result of the large ring strain energy (RSE) in the

573   cyclic transition state geometries. As a consequence, the isomerization reactions of

574   HOCH$_2$OO, HOCH(CH$_3$)OO and HO(CH$_3$)$_2$COO radicals are not likely to proceed in

575   the atmosphere.

576   The single-conformer rate coefficients ($k_{IRC-TST}$) and multi-conformer rate

577   coefficients (k_{MC-TST}) of the isomerization of HOCH$_2$OO, HOCH(CH$_3$)OO and

578   HOC(CH$_3$)$_2$OO radicals are calculated over the temperature range of 273-400 K as

579   listed in Table S9-S11. As can be seen in Table S9, $k_{IRC-TST}$ of each conformer exhibits

580   a marked positive temperature dependence over the temperature range studied.

581   k_{MC-TST} is significantly increased with rising temperature, implying that the

582   temperature increasing is beneficial to the occurrence of HOCH$_2$OO radical

583   isomerization. Similar conclusion is also obtained from the isomerization of

584   HOCH(CH$_3$)OO and HOC(CH$_3$)$_2$OO radicals (Table S10-S11). It is worth mentioning

585   that k_{MC-TST} is rapidly increased as the number of methyl group is increased. For

586 example, the room temperature $k_{MC\text{-}TST}$ of HOCH$_2$OO radical isomerization is
587 calculated to be 4.4×10^{-16} s^{-1}, which is lower than those of the HOCH(CH$_3$)OO (2.9
588 $\times 10^{-13}$ s^{-1}) and HO(CH$_3$)$_2$COO (3.0×10^{-12} s^{-1}) radicals isomerization by 660 and
589 6820 times, respectively.
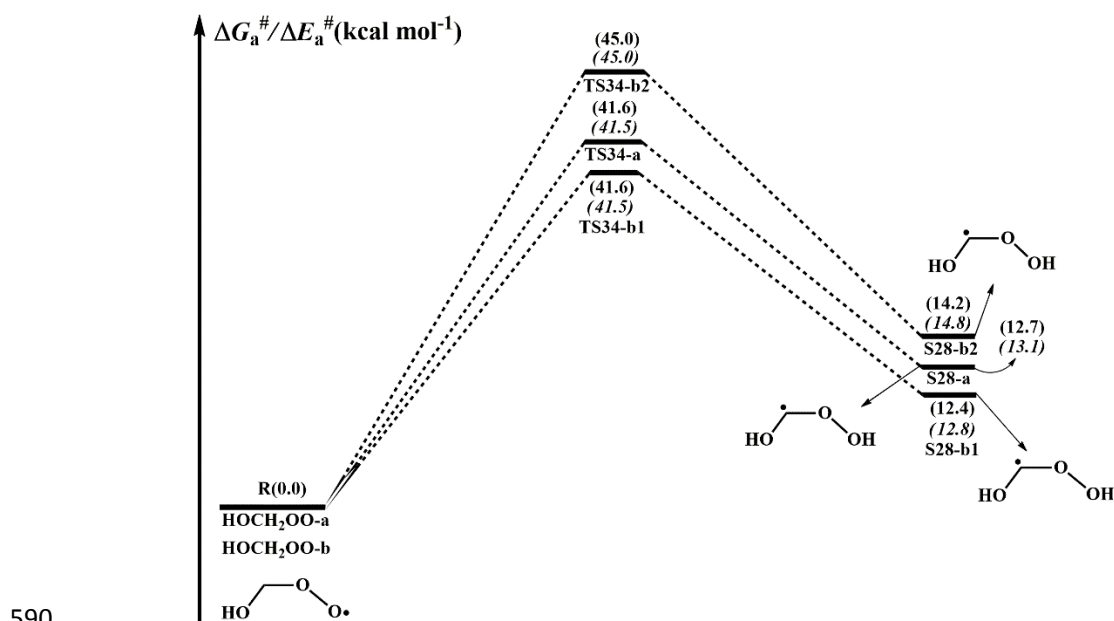
590
591 **Figure 9.** PES ($\Delta G_a^{\#}$ and $\Delta E_a^{\#}$, in italics) for the isomerization of HOCH$_2$OO radical predicted at
592 the M06-2X/ma-TZVP//M06-2X/6-311+G(2df,2p) level of theory

3.3 Subsequent reactions of H-abstraction products RO$_2$ radicals in urban environments

595   NO$_x$ is present in high concentration in urban environments, reaction with NO is
596 the dominant chemical sink for RO$_2$ radicals (Atkinson and Arey, 2003; Orlando and
597 Tyndall, 2012; Perring et al., 2013). The main pathways in this type of reaction lead to
598 the formation of NO$_2$, RO radicals, organic nitrites, and organic nitrate, and their
599 formation yields are highly dependent on the nature of R group (Orlando and Tyndall,
600 2012). The formation of NO$_2$ through subsequent photolysis ($\lambda < 420$ nm) produces
601 ozone and NO, increasing the concentrations of near-surface ozone and propagating
602 NO$_x$ chain (Orlando and Tyndall, 2012). The schematic PES for the reactions of
603 distinct RO$_2$ radicals with NO are displayed in Figures 10-12. As shown in Figure 10,
604 the bimolecular reaction between HOCH$_2$OO radical and NO initially leads to nitrite
605 adduct S31 via the barrierless addition of NO to terminal oxygen atom O$_3$ of
606 HOCH$_2$OO radical. The formed S31 exists two isomers: S31-*cis* refers to the O$_2$ and

607   O_4 on the same side ($DO_2O_3N_1O_4 = 2.3 °$), whereas S31-*trans* refers to the O_2 and O_4

608   on the opposite side ($DO_2O_3N_1O_4 = -179.8 °$) with respect to the O_3-N_1 bond. The

609   calculations show that S31-*cis* is more stable than S31-*trans* by 1.1 kcal·mol^{-1} in

610   energy. The tautomerization between S31-*cis* and S31-*trans* proceeds through the

611   rotating of O_3-N_1 bond with the barrier of 14.4 kcal·mol^{-1}, implying that they can be

612   regarded as the separate atmospheric species. According to the Boltzmann-weighted

613   distribution, at room temperature, the predicted percentages of S31-*cis* and S31-*trans*

614   are 86.5% and 13.5%, respectively. The result implies that the dominant product of

615      $HOCH_2OO$ radical reaction with NO is S31-*cis*, and it is selected as a model

616   compound to insight into the mechanism of secondary reactions in the following

617   sections.

618   S31-*cis* can either isomerize to organic nitrate S32 (R38) via the O_2-O_3 bond

619   breaking and O_2-N_1 bond forming with the barrier of 47.8 kcal·mol^{-1}, or decompose

620   into $HOCH_2O$ radical and NO_2 (R39) via the cleavage of O_2-O_3 bond with the barrier

621   of 11.3 kcal·mol^{-1}. The result shows that the latter pathway is more favourable than

622   the former channel due to its lower barrier. It should be noted that the corresponding

623   transition state TS39 is not located using M06-2X functional, but it is located at the

624   MP2/6-311+G(2df,2p) level of theory and is verified using IRC calculations. The

625   formed $HOCH_2O$ radical has two kinds of pathways: (1) it directly decomposes into

626   CH_2O and OH radical (R40) via β-site C_1-O_1 bond scission with the barrier of 52.4

627   kcal·mol^{-1}; (2) it converts into HCOOH and HO_2 radical (R41) through H-abstraction

628   by O_2 with the barrier of 26.4 kcal·mol^{-1}. This result reveals that R41 is the most

629   feasible channel in the fragmentation of $HOCH_2O$ radical.

630   From Figure 11, it can be seen that the addition NO to $HOCH(CH_3)OO$ radical

631   leading to the formation of S33-*cis* is barrierless. Then, it decomposes into

632      $HOCH(CH_3)O$ radical and NO_2 (R44) via the cleavage of O_2-O_3 bond with the barrier

633   of 11.5 kcal·mol^{-1}. The resulting $HOCH(CH_3)O$ radical has three types of pathways.

634   The first one is β-site C_1-C_2 bond scission leading to the formation of HCOOH +

635   CH_3 (R45) with the barrier of 8.3 kcal·mol^{-1}. The second one is β-site C_1-O_1 bond

636   cleavage resulting in formation of CH_3COH + OH (R46) with the barrier of 26.7

637 kcal mol^{-1}. The third one is H-abstraction by O_2 leading to $CH_3COOH + HO_2 \cdot$ (R47)

638 with the barrier of 26.2 kcal mol^{-1}. Based on the calculated reaction barriers, it can be

639 found that β-site C_1-C_2 bond scission is the dominant pathway in the fragmentation of

640 HOCH(CH$_3$)O radical. This conclusion is further supported by the previous

641 experimental result that β-hydroxy intermediates primarily proceed decomposition

642 rather than react with O_2 in the presence of NO (Aschmann et al., 2000). Equivalent to

643 the HOCH(CH$_3$)OO $\cdot$ + NO reaction, the bimolecular reaction of HO(CH$_3$)$_2$COO

644 radical with NO has similar transformation pathways (Figure 12). The reaction for

645 HO(CH$_3$)$_2$COO with NO initially proceeds via a barrierless addition leading to

646 S35-cis with the binding energy of 12.6 kcal mol^{-1}. Then, S35-cis fragments into

647 HO(CH$_3$)$_2$CO radical along with NO_2 (R50) via the cleavage of O_2-O_3 bond with the

648 barrier of 11.4 kcal mol^{-1}. The formed HO(CH$_3$)$_2$CO radical can either dissociate to

649 $CH_3COOH + CH_3 \cdot$ (R51) via the C_1-C_3 bond scission with the barrier of 8.2

650 kcal mol^{-1}, or decompose into $CH_3COCH_3 + $ OH (R52) through the C_1-O_1 bond

651 breaking with the barrier of 24.3 kcal mol^{-1}. The result again shows that the β-site

652 C-C bond scission is the dominate pathway.

653 The typical atmospheric concentrations of NO are about 10 ppbv, 1 ppbv and 20

654 pptv in the urban, rural and forest environments (Bianchi et al., 2019). The rate

655 coefficient of HOCH$_2$OO $\cdot$ reaction with NO is calculated to be 4.3 $\times$ 10^{-12} cm^3

656 molecule^{-1} s^{-1} at room temperature, resulting in the pseudo-first-order rate constants

657 $k'_{NO} = k_{NO}$[NO] of 6.5 $\times$ 10^{-1}, 6.5 $\times$ 10^{-2}, and 1.3 $\times$ 10^{-3}, respectively, in the urban,

658 rural and forest environments. It is of interest to assess the relative importance for the

659 H-shift reaction of HOCH$_2$OO radical and bimolecular reactions with HO$_2$ $\cdot$ and NO

660 based on the calculated k_{MC-TST}, k'_{HO2} and k'_{NO}. It can be found that the H-shift

661 reaction is of less importance, the HO$_2$ radical reaction is favorable in the forest

662 environment, while the NO reaction is predominant in the urban and rural regions.

663 Similar conclusion is also obtained from the cases of HOCH(CH$_3$)OO and

664 HO(CH$_3$)$_2$CHOO radicals.

665 The rate coefficients of the dominant pathways of HOCH$_2$O, HOCH(CH$_3$)O and

666 HO(CH$_3$)$_2$CHO radicals fragmentation are summarized in Table S12. As can be seen

667   in Table S12, k_{R41} is slightly increased with the temperature increasing, and the

668   discrepancy is about a factor of 12 at the two extremes of temperature. At ground

669   level with $[O_2] = \sim 5.0 \times 10^{18}$ molecule cm^{-3}, the pseudo-first-order rate constant k'_{O2}

670    $= k_{R41}[O_2]$ is estimated to be 38.0 s^{-1} at room temperature. k_{R45} vary significantly from

671   2.0×10^6 (273 K) to 3.1×10^8 (400 K) s^{-1}, and they exhibit a marked positive

672   temperature dependence. Similar phenomenon is also observed from k_{R51} that k_{R51} is

673   significantly increased with increasing temperature. k_{R51} is a factor of ~ 1.3 greater

674   than k_{R45} in the temperature range studied, implying that the rate coefficient of β-site

675   C-C bond scission is slightly increased as the number of methyl group is increased.
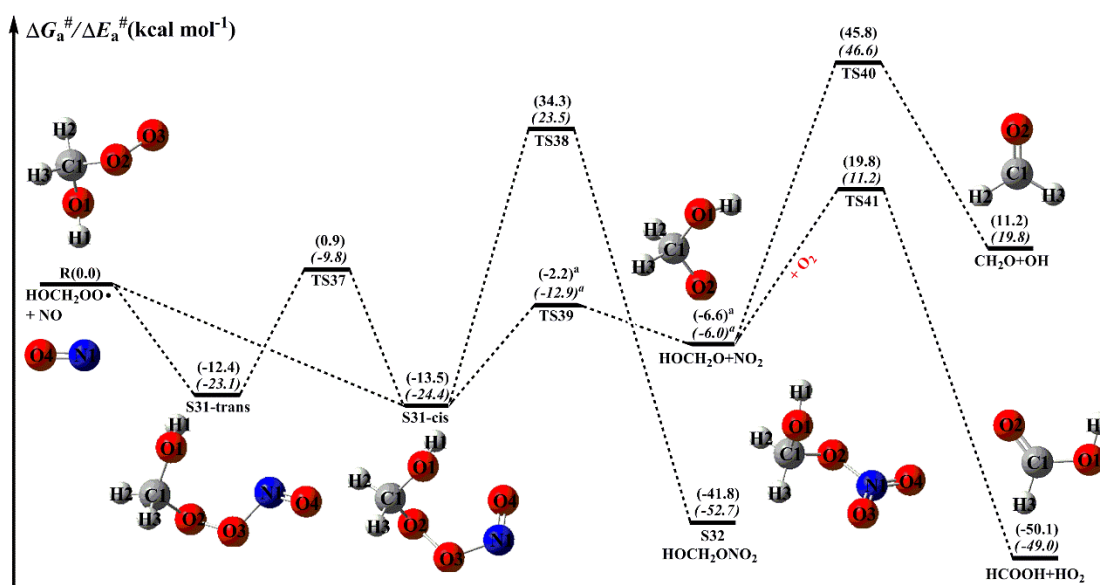
Figure 10. PES ($\Delta G_a^{\#}$ and $\Delta E_a^{\#}$, in italics) for the reaction of HOCH$_2$OO radical with NO predicted at the M06-2X/ma-TZVP//M06-2X/6-311+G(2df,2p) level of theory (the superscript a is calculated at the MP2/ma-TZVP//MP2/6-311+G(2df,2p) level)
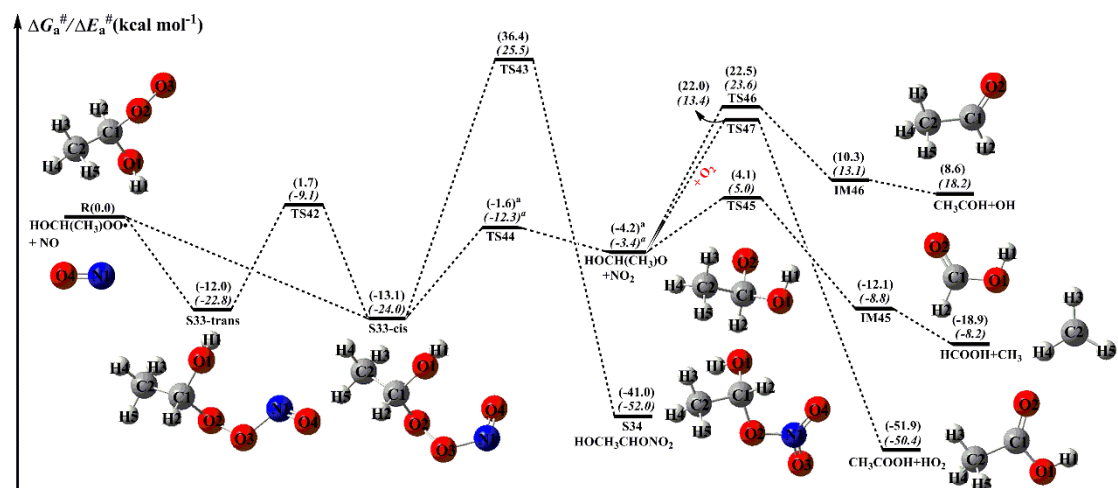
Figure 11. PES ($\Delta G_a^{\#}$ and $\Delta E_a^{\#}$, in italics) for the reaction of HOCH(CH$_3$)OO radical with NO predicted at the M06-2X/ma-TZVP//M06-2X/6-311+G(2df,2p) level of theory (the superscript a is calculated at the MP2/ma-TZVP//MP2/6-311+G(2df,2p) level)
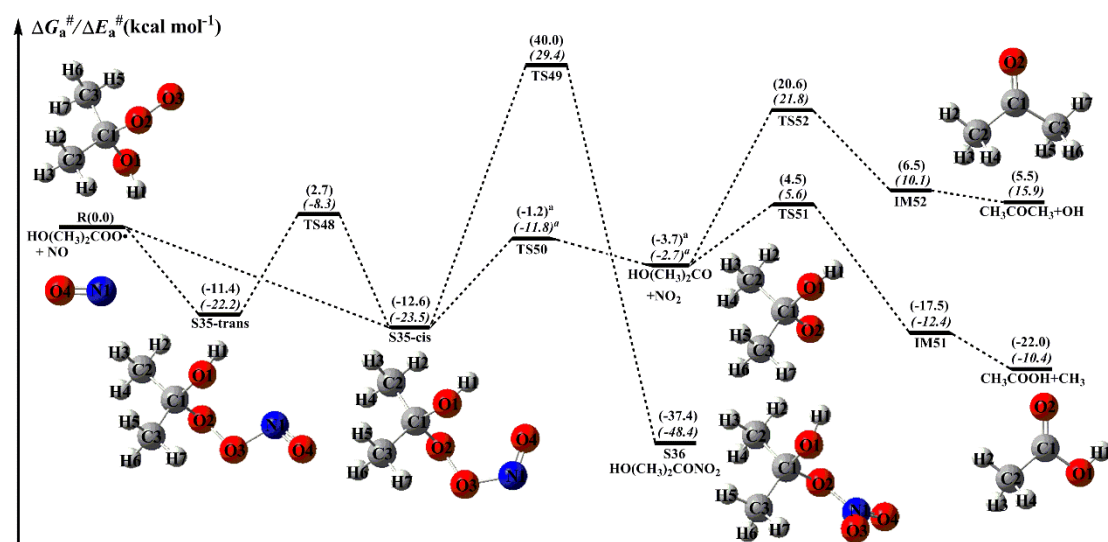
Figure 12. PES ($\Delta G_a^{\#}$ and $\Delta E_a^{\#}$, in italics) for the reaction of HO(CH$_3$)$_2$COO radical with NO predicted at the M06-2X/ma-TZVP//M06-2X/6-311+G(2df,2p) level of theory (the superscript a is calculated at the MP2/ma-TZVP//MP2/6-311+G(2df,2p) level)

4. Conclusions

The detailed mechanisms and kinetic properties of OH-initiated oxidation of distinct HHPs and subsequent transformation of resulting H-abstraction products are investigated using quantum chemical and kinetics modeling methods. The main conclusions are summarized as follows:

(a) The dominant pathway is the H-abstraction from the -OOH group in the initiation reactions of OH radical with HOCH$_2$OOH and HOC(CH$_3$)$_2$OOH. H-abstraction from -CH group is competitive with that from the -OOH group in the

698 reaction of OH radical with HOCH(CH$_3$)OOH. The barrier of H-abstraction from the

699 -OOH group is slightly increased as the number of methyl group is increased.

700 Compared with the rate coefficient of dominant pathway in the parent system, it is

701 almost identical when a methyl group substitution occurs at the C$_1$-position, whereas

702 it reduces by a factor of 2-5 when two methyl groups introduce into the C$_1$-position.

703   (b) The self-reaction of H-abstraction product RO$_2$ radical initially produces

704 tetroxide intermediate via an oxygen-to-oxygen coupling, then it decomposes into

705 propagation and termination products through the asymmetric two-step O-O bond

706 scission. The rate-limiting step is the first O-O bond cleavage, and the barrier is

707 increased with increasing the number of methyl group.

708   (c) The bimolecular reactions of distinct RO$_2$ radicals with HO$_2$ radical lead to

709 the formation of hydroperoxide ROOH as the main product, and the barrier height is

710 independent on the number of methyl substitution. The calculated rate coefficients

711 exhibit a weakly negative temperature dependence, translating into the

712 pseudo-first-order rate constant k'_{HO2} of 1-5 $\times 10^{-2}$ s^{-1} in the forest environments.

713   (d) Reaction with O$_2$ forming formic acid and HO$_2$ radical is the dominant

714 removal pathway for HOCH$_2$O radical formed from the reaction of HOCH$_2$OO

715 radical with NO. The β-site C-C bond scission is the dominate pathway in the

716 dissociation of HOCH(CH$_3$)O and HOC(CH$_3$)$_2$O radicals formed from the

717 HOCH(CH$_3$)OO $\cdot$+ NO and HOC(CH$_3$)$_2$OO $\cdot$+ NO reactions.

718

Data availability

720   The data are accessible by contacting the corresponding author

721 (huangyu@ieecas.cn).

722

Supplement

724   The following information is provided in the Supplement: Y//X (Y = M06-2X,

725 CCSD(T), X = 6-311+G(2df,2p), ma-TZVP) calculated energy barrier ($\Delta E_a^{\#}$, $\Delta G_a^{\#}$)

726 for OH + HHPs reactions; Rate coefficients of every elementary pathway involved in

the initial reactions of OH radical with $HOCH_2OOH$, $HOCH(CH_3)OOH$ and $HO(CH_3)_2COOH$; Rate coefficients of HO_2 radical reactions with $HOCH_2OO$, $HOCH(CH_3)OO$ and $HO(CH_3)_2COO$ radicals; The relative free energy and Boltzmann populations (w_i) of the conformer of $HOCH_2OO$, $HOCH(CH_3)OO$ and $HO(CH_3)_2COO$ radicals; The single-conformer rate coefficients ($k_{IRC-TST}$) and multi-conformer rate coefficients (k_{MC-TST}) of $HOCH_2OO$, $HOCH(CH_3)OO$ and $HO(CH_3)_2COO$ radicals; Rate coefficients of dominant pathways in the $HOCH_2OO \cdot + NO$, $HOCH(CH_3)OO \cdot + NO$ and $HO(CH_3)_2CHOO \cdot + NO$ reactions; PESs ($\Delta E_a^{\#}$) for the OH-initiated reactions of $HOCH_2OOH$, $HOCH(CH_3)OOH$, $HOC(CH_3)_2OOH$; Geometries of all the stationary points; Plots of the rate coefficients of every elementary pathway versus temperature; PESs ($\Delta G_a^{\#}$ and $\Delta E_a^{\#}$, in italics) for the isomerization of $HOCH(CH_3)OO$ and $HO(CH_3)_2COO$ radicals.

Author contribution

LC designed the study. LC and YH wrote the paper. LC performed theoretical calculation. YX, ZJ, and WW analyzed the data. All authors reviewed and commented on the paper.

Competing interests

The authors declare that they have no conflict of interest.

Acknowledgments

This work was supported by the National Natural Science Foundation of China (grant Nos. 42175134, 41805107, and 22002080). It was also partially supported as Key Projects of Chinese Academy of Sciences, China (grant No. ZDRW-ZS-2017-6), Strategic Priority Research Program of the Chinese Academy of Sciences, China (grant Nos. XDA23010300 and XDA23010000), Key Project of International Cooperation of the Chinese Academy of Sciences, China (grant No. GJHZ1543),

Research Grants Council of Hong Kong, China (grant No. PolyU 152083/14E), CAS "Light of West China" Program (XAB2019B01) and the General Project of Shaanxi Province (2020JQ-432).

References

Allen, H. M., Crounse, J. D., Bates, K. H., Teng, A. P., Krawiec-Thayer, M. P., Rivera-Rios, J. C., Keutsch, F. N., Clair, J. M. S., Hanisco, T. F., Møller, K. H., Kjaergaard, H. G., and Wennberg, P. O.: Kinetics and product yields of the OH initiated oxidation of hydroxymethyl hydroperoxide, J. Phys. Chem. A, 122, 6292-6302, https://doi.org/10.1021/acs.jpca.8b04577, 2018.

Anglada, J. M., and Solé, A.: Impact of the water dimer on the atmospheric reactivity of carbonyl oxides, Phys. Chem. Chem. Phys., 18, 17698-17712, https://doi.org/10.1039/C6CP02531E, 2016.

Anglada, J. M., González, J., and Torrent-Sucarrat, M.: Effects of the substituents on the reactivity of carbonyl oxides. a theoretical study on the reaction of substituted carbonyl oxides with water, Phys. Chem. Chem. Phys., 13, 13034-13045, https://doi.org/10.1039/c1cp20872a, 2011.

Aschmann, S. M., Arey, J., and Atkinson, R.: Formation of β-hydroxycarbonyls from the OH radical-initiated reactions of selected alkenes, Environ. Sci. Technol., 34, 1702-1706, https://doi.org/10.1021/es991125a, 2000.

Atkinson, R., and Arey, J.: Atmospheric degradation of volatile organic compounds, Chem. Rev., 103, 4605-4638, https://doi.org/10.1021/cr0206420, 2003.

Bach, R. D., Dmitrenko, O., and Estévez, C. M.: Chemical behavior of the biradicaloid (HO $\cdots$ ONO) singlet states of peroxynitrous acid. the oxidation of hydrocarbons, sulfides, and selenides, J. Am. Chem. Soc., 127, 3140-3155, https://doi.org/10.1021/ja044245d, 2005.

Berndt, T., Richters, S., Kaethner, R., Voigtländer, J., Stratmann, F., Sipilä, M., Kulmala, M., and Herrmann, H.: Gas-phase ozonolysis of cycloalkenes: formation of highly oxidized RO_2 radicals and their reactions with NO, NO_2, SO_2, and Other RO_2 radicals, J. Phys. Chem. A, 119, 10336-10348, https://doi.org/10.1021/acs.jpca.5b07295, 2015.

Berndt, T., Scholz, W., Mentler, B., Fischer, L., Herrmann, H., Kulmala, M., and Hansel, A.: Accretion product formation from self- and cross-reactions of RO_2 radicals in the atmosphere, Angew. Chem. Int. Ed., 57, 3820-3824, https://doi.org/10.1002/anie.201710989, 2018.

Bianchi, F., Kurten, T., Riva, M., Mohr, C., Rissanen, M. P., Roldin, P., Berndt, T., Crounse, J. D., Wennberg, P. O., Mentel, T. F., Wildt, J., Junninen, H., Jokinen, T., Kulmala, M., Worsnop, D. R., Thornton, J. A., Donahue, N., Kjaergaard, H. G., and Ehn, M.: Highly oxygenated organic molecules (HOM) from gas-phase autoxidation involving peroxy radicals: a key contributor to atmospheric aerosol, Chem. Rev., 119, 3472-3509, https://doi.org/10.1021/acs.chemrev.8b00395, 2019.

Boys, S. F., and Bernardi, F.: The calculation of small molecular interactions by the differences of separate total energies. Some procedures with reduced errors, Mol. Phys., 19, 553-566, https://doi.org/10.1080/00268977000101561, 1970.

Chao, W., Hsieh, J. T., Chang, C. H., and Lin, J. J. M.: Direct kinetic measurement of the reaction of the simplest Criegee intermediate with water vapor, Science, 347, 751-754, https://doi.org/10.1126/science.1261549, 2015.

Chen, L., Huang, Y., Xue, Y., Cao, J., and Wang, W.: Competition between HO_2 and H_2O_2 reactions with CH_2OO/*anti*-CH_3CHOO in the oligomer formation: a theoretical perspective, J. Phys. Chem. A, 121, 6981-6991, https://doi.org/10.1021/acs.jpca.7b05951, 2017.

Chen, L., Huang, Y., Xue, Y., Jia, Z., and Wang, W.: Atmospheric oxidation of 1-butene initiated by OH radical: Implications for ozone and nitrous acid formations, Atmos. Environ., 244, 118010-118021, https://doi.org/10.1016/j.atmosenv.2020.118010, 2021.

Chen, L., Huang, Y., Xue, Y., Shen, Z., Cao, J., and Wang, W.: Mechanistic and kinetics investigations of oligomer formation from Criegee intermediate reactions with hydroxyalkyl hydroperoxides, Atmos. Chem. Phys., 19, 4075-4091, https://doi.org/10.5194/acp-19-4075-2019, 2019.

Chen, L., Wang, W., Wang, W., Liu, Y., Liu, F., Liu, N., and Wang, B.: Water-catalyzed decomposition of the simplest Criegee intermediate CH_2OO, Theor. Chem. Acc., 135, 131-143, https://doi.org/10.1007/s00214-016-1894-9, 2016b.

Chen, L., Wang, W., Zhou, L., Wang, W., Liu, F., Li, C., and Lü, J.: Role of water clusters in the reaction of the simplest Criegee intermediate CH_2OO with water vapour, Theor. Chem. Acc., 135, 252-263, https://doi.org/10.1007/s00214-016-1998-2, 2016a.

Chhantyal-Pun, R., Welz, O., Savee, J. D., Eskola, A. J., Lee, E. P. F., Blacker, L., Hill, H. R., Ashcroft, M., Khan, M. A. H., Lloyd-Jones, G. C., Evans, L., Rotavera, B., Huang, H., Osborn, D. L., Mok, D. K. W., Dyke, J. M., Shallcross, D. E., Percival, C. J., Orr-Ewing, A. J., and Taatjes, C. A.: Direct measurements of unimolecular and bimolecular reaction kinetics of the Criegee intermediate $(CH_3)_2COO$, J. Phys. Chem. A, 121, 4-15, https://doi.org/10.1021/acs.jpca.6b07810, 2017.

Crounse, J. D., Nielsen, L. B., Jørgensen, S., Kjaergaard, H. G., and Wennberg, P. O.: Autoxidation of organic compounds in the atmosphere, J. Phys. Chem. Lett., 4, 3513-3520, https://doi.org/10.1021/jz4019207, 2013.

Dillon, T. J., and Crowley, J. N.: Direct detection of OH formation in the reactions of HO_2 with $CH_3C(O)O_2$ and other substituted peroxy radicals, Atmos. Chem. Phys., 8, 4877-4889, https://doi.org/10.5194/acp-8-4877-2008, 2008.

Eckart, C.: The penetration of a potential barrier by electrons, Phys. Rev., 35, 1303-1309, https://doi.org/10.1103/PhysRev.35.1303, 1930.

Ehn, M., Berndt, T., Wildt, J., and Mentel, T.: Highly oxygenated molecules from atmospheric autoxidation of hydrocarbons: a prominent challenge for chemical kinetics studies, Int. J. Chem. Kinet., 49, 821-831, https://doi.org/10.1002/kin.21130, 2017.

Ehn, M., Thornton, J. A., Kleist, E., Sipilä, M., Junninen, H., Pullinen, I., Springer, M., Rubach, F., Tillmann, R., Lee, B., Lopez-Hilfiker, F., Andres, S., Acir, I. H., Rissanen, M., Jokinen,T., Schobesberger, S., Kangasluoma, J., Kontkanen, J., Nieminen, T., Kurtén, T., Nielsen, L. B., Jørgensen, S., Kjaergaard, H. G., Canagaratna, M., Maso, M. D., Berndt, T., Petäjä, T., Wahner, A., Kerminen, V. M., Kulmala, M., Worsnop, D. R., Wildt, J., and Mentel T. F.: A large source of low-volatility secondary organic aerosol, Nature, 506, 476-479, https://doi.org/10.1038/nature13032, 2014.

Fernández-Ramos, A., Ellingson, B. A., Meana-Pañeda, R., Marques, J. M. C., and Truhlar, D. G.:

Symmetry numbers and chemical reaction rates, Theor. Chem. Acc., 118, 813-826, https://doi.org/10.1007/s00214-007-0328-0, 2007.

Francisco, J. S., and Eisfeld, W.: Atmospheric oxidation mechanism of hydroxymethyl hydroperoxide, J. Phys. Chem. A, 113, 7593-7600, https://doi.org/10.1021/jp901735z, 2009.

Frisch, M. J., Trucks, G. W., Schlegel, H. B., Scuseria, G. E., Robb, M. A., Cheeseman, J. R., Montgomery, J. A. Jr., Vreven, T., Kudin, K. N., Burant, J. C., Millam, J. M., Iyengar, S. S., Tomasi, J., Barone, V., Mennucci. B., Cossi, M., Scalmani, G., Rega, N., Petersson, G. A., Nakatsuji, H., Hada, M., Ehara, M., Toyota, K., Fukuda, R., Hasegawa, J., Ishida, M., Nakajima, T., Honda, Y., Kitao, O., Nakai, H., Klene, M., Li, X., Knox, J. E., Hratchian, H. P., Cross, J. B., Adamo, C., Jaramillo, J., Gomperts, R., Stratmann, R. E., Yazyev, O., Austin, A. J., Cammi, R., Pomelli, C., Ochterski, J. W., Ayala, P. Y., Morokuma, K., Voth, G. A., Salvador, P., Dannenberg, J. J., Zakrzewski, V. G., Dapprich, S., Daniels, A. D., Strain, M. C., Farkas, O., Malick, D. K., Rabuck, A. D., Raghavachari, K., Foresman, J. B., Ortiz, J. V., Cui, Q., Baboul, A. G., Clifford, S., Cioslowski, J., Stefanov, B. B., Liu, G., Liashenko, A., Piskorz, P., Komaromi, I., Martin, R. L., Fox, D. J., Keith, T., Al-Laham, M. A., Peng, C. Y., Nanayakkara, A., Challacombe, M., Gill, P. M. W., Johnson, B., Chen, W., Wong, M. W., Gonzalez, C., and Pople, J. A.: Gaussian 09, Revision D.01; Gaussian, Inc.: Wallingford, CT, 2009.

Fukui, K.: The path of chemical reactions - the IRC approach, Acc. Chem. Res., 14, 363-368, https://doi.org/10.1021/ar00072a001, 1981.

Gilbert, R. G., and Smith, S. C.: Theory of unimolecular and recombination reactions; Blackwell Scientific: Carlton, Australia, 1990.

Gligorovski, S., Strekowski, R., Barbati, S., and Vione, D.: Environmental implications of hydroxyl radicals (OH), Chem. Rev., 115, 13051-13092, https://doi.org/10.1021/cr500310b, 2015.

Glowacki, D. R., Liang, C. H., Morley, C., Pilling, M. J., and Robertson, S. H.: MESMER: an open-source master equation solver for multi-energy well reactions, J. Phys. Chem. A, 116, 9545-9560, https://doi.org/10.1021/jp3051033, 2012.

Gong, Y., and Chen, Z.: Quantification of the role of stabilized Criegee intermediates in the formation of aerosols in limonene ozonolysis, Atmos. Chem. Phys., 21, 813-829, https://doi.org/10.5194/acp-21-813-2021, 2021.

Hofzumahaus, A., Rohrer, F., Lu, K., Bohn, B., Brauers, T., Chang, C. C., Fuchs, H., Holland, F., Kita, K., Kondo, Y., Li, X., Lou, S., Shao, M., Zeng, L., Wahner, A., and Zhang, Y.: Amplified trace gas removal in the troposphere, Science, 324, 1702-1704, https://doi.org/10.1126/science.1164566, 2009.

Holbrook, K. A., Pilling, M. J., Robertson, S. H., and Robinson, P. J.: Unimolecular reactions, 2nd ed.; Wiley: New York, 1996.

Huang, H. L., Chao, W., and Lin, J. J. M.: Kinetics of a Criegee intermediate that would survive high humidity and may oxidize atmospheric SO_2, Proc. Natl. Acad. Sci. U.S.A., 112, 10857-10862, https://doi.org/10.1073/pnas.1513149112, 2015.

Iyer, S., Reiman, H., Møller, K. H., Rissanen, M. P., Kjaergaard, H. G., and Kurtén, T.: Computational investigation of $RO_2 + HO_2$ and $RO_2 + RO_2$ reactions of monoterpene derived first-generation peroxy radicals leading to radical recycling, J. Phys. Chem. A, 122, 9542-9552, https://doi.org/10.1021/acs.jpca.8b09241, 2018.

884 Iyer, S., Rissanen, M. P., Valiev, R., Barua, S., Krechmer, J. E., Thornton, J., Ehn, M., and Kurtén,
885   T.: Molecular mechanism for rapid autoxidation in α-pinene ozonolysis, Nat. Commun.,
886   https://doi.org/10.1038/s41467-021-21172-w, 12, 878-883, 2021.

887 Jara-Toro, R. A., Hernández, F. J., Garavagno, M. A., Taccone, R. A., and Pino, G. A.: Water
888   catalysis of the reaction between hydroxyl radicals and linear saturated alcohols (ethanol and
889   n-propanol) at 294 K, Phys. Chem. Chem. Phys., 20, 27885-27896,
890   https://doi.org/10.1039/C8CP05411H, 2018.

891 Jara-Toro, R. A., Hernández, F. J., Taccone, R. A., Lane, S. I., and Pino, G. A.: Water catalysis of
892   the reaction between methanol and OH at 294 K and the atmospheric implications, Angew.
893   Chem., Int. Ed., 56, 2166-2170, https://doi.org/10.1002/anie.201612151, 2017.

894 Jokinen, T., Sipilä, M., Richters, S., Kerminen, V. M., Paasonen, P., Stratmann, F., Worsnop, D.,
895   Kulmala, M., Ehn, M., Herrmann, H., and Berndt, T.: Rapid autoxidation forms highly
896   oxidized RO_2 radicals in the atmosphere, Angew. Chem. Int. Ed., 53, 14596-14600,
897   https://doi.org/10.1002/anie.201408566, 2014.

898 Khan, M. A. H., Percival, C. J., Caravan, R. L., Taatjes, C. A., and Shallcross, D. E.: Criegee
899   intermediates and their impacts on the troposphere, Environ. Sci.: Processes Impacts, 20,
900   437-453, https://doi.org/10.1039/C7EM00585G, 2018.

901 Kumar, M., and Francisco, J. S.: Red-light initiated decomposition of α-hydroxy methylperoxy
902   radical in the presence of organic and inorganic acids: implications for the HO_x formation in
903   the lower stratosphere, J. Phys. Chem. A, 120, 2677-2683,
904   https://doi.org/10.1021/acs.jpca.6b01515, 2016.

905 Kumar, M., and Francisco, J. S.: Red-light-induced decomposition of an organic peroxy radical: a
906   new source of the HO_2 radical, Angew. Chem. Int. Ed., 54, 15711-15714,
907   https://doi.org/10.1002/anie.201509311, 2015.

908 Kumar, M., Busch, D. H., Subramaniam, Bala., and Thompson, W. H.: Role of tunable acid
909   catalysis in decomposition of α-hydroxyalkyl hydroperoxides and mechanistic implications
910   for tropospheric chemistry, J. Phys. Chem. A, 118, 9701-9711,
911   https://doi.org/10.1021/jp505100x, 2014.

912 Lee, R., Gryn'ova, G., Ingold, K. U., and Coote, M. L.: Why are sec-alkylperoxyl bimolecular
913   self-reactions orders of magnitude faster than the analogous reactions of tert-alkylperoxyls?
914   The unanticipated role of CH hydrogen bond donation, Phys. Chem. Chem. Phys., 18,
915   23673-23679, https://doi.org/10.1039/C6CP04670C, 2016.

916 Lester, M. I., and Klippenstein, S. J.: Unimolecular decay of Criegee intermediates to OH radical
917   products: prompt and thermal decay processes, Acc. Chem. Res., 51, 978-985,
918   https://doi.org/10.1021/acs.accounts.8b00077, 2018.

919 Liu, L., Bei, N., Wu, J., Liu, S., Zhou, J., Li, X., Yang, Q., Feng, T., Cao, J., Tie, X., and Li, G.:
920   Effects of stabilized Criegee intermediates (sCIs) on sulfate formation: a sensitivity analysis
921   during summertime in Beijing-Tianjin-Hebei (BTH), China. Atmos. Chem. Phys., 19,
922   13341-13354, https://doi.org/10.5194/acp-19-13341-2019, 2019.

923 Long, B., Bao, J. L., and Truhlar, D. G.: Reaction of SO_2 with OH in the atmosphere, Phys. Chem.
924   Chem. Phys., 19, 8091-8100, https://doi.org/10.1039/C7CP00497D, 2017.

925 Lu, T.: Molclus program, Version 1.9.3, http://www.keinsci.com/research/molclus.html (accessed
926   Feb. 10, 2020).

927 Ma, F., Guo, X., Xia, D., Xie, H. B., Wang, Y., Elm, J., Chen, J., and Niu, J.: Atmospheric

chemistry of allylic radicals from isoprene: a successive cyclization-driven autoxidation mechanism, Environ. Sci. Technol., 55, 4399-4409, https://doi.org/10.1021/acs.est.0c07925, 2021.

Møller, K. H., Berndt, T., and Kjaergaard, H. G.: Atmospheric autoxidation of amines, Environ. Sci. Technol., 54, 11087-11099, https://doi.org/10.1021/acs.est.0c03937, 2020.

Møller, K. H., Otkjær, R. V., Hyttinen, N., Kurtén, T., and Kjaergaard, H. G.: Cost-effective implementation of multiconformer transition state theory for peroxy radical hydrogen shift reactions, J. Phys. Chem. A, 120, 10072-10087, https://doi.org/10.1021/acs.jpca.6b09370, 2016.

Nozière, B., and Vereecken, L.: Direct observation of aliphatic peroxy radical autoxidation and water effects: an experimental and theoretical study, Angew. Chem. Int. Ed., 58, 13976-13982, https://doi.org/10.1002/anie.201907981, 2019.

Orlando, J. J., and Tyndall, G. S.: Laboratory studies of organic peroxy radical chemistry: an overview with emphasis on recent issues of atmospheric significance, Chem. Soc. Rev., 41, 6294-6317, https://doi.org/10.1039/c2cs35166h, 2012.

Perring, A. E., Pusede, S. E., and Cohen, R. C.: An observational perspective on the atmospheric impacts of alkyl and multifunctional nitrates on ozone and secondary organic aerosol, Chem. Rev., 113, 5848-5870, https://doi.org/10.1021/cr300520x, 2013.

Qiu, J. T., Ishizuka, S., Tonokura, K., Colussi, A. J., and Enami, S.: Water dramatically accelerates the decomposition of α-hydroxyalkyl-hydroperoxides in aerosol particles, J. Phys. Chem. Lett., 10, 5748-5755, https://doi.org/10.1021/acs.jpclett.9b01953, 2019.

Rissanen, M. P., Kurtén, T., Sipilä, M., Thornton, J. A., Kangasluoma, J., Sarnela, N., Junninen, H., Jørgensen, S., Schallhart, S., Kajos, M. K., Taipale, R., Springer, M., Mentel, T. F., Ruuskanen, T., Petäjä, T., Worsnop, D. R., Kjaergaard, H. G., and Ehn, M.: The formation of highly oxidized multifunctional products in the ozonolysis of cyclohexene, J. Am. Chem. Soc., 136, 15596-15606, https://doi.org/10.1021/ja507146s, 2014.

Russell, G. A.: Deuterium-isotope effects in the autoxidation of aralkyl hydrocarbons. Mechanism of the interaction of peroxy radicals, J. Am. Chem. Soc., 79, 3871-3877, https://doi.org/10.1021/ja01571a068, 1957.

Ryzhkov, A. B., and Ariya, P. A.: A theoretical study of the reactions of carbonyl oxide with water in atmosphere: the role of water dimer, Chem. Phys. Lett., 367, 423-429, https://doi.org/10.1016/S0009-2614(02)01685-8, 2003.

Smith, M. C., Chang, C. H., Chao, W., Lin, L. C., Takahashi, K., Boering, K. A., and Lin, J. J. M.: Strong negative temperature dependence of the simplest Criegee intermediate CH_2OO reaction with water dimer, J. Phys. Chem. Lett., 6, 2708-2713, https://doi.org/10.1021/acs.jpclett.5b01109, 2015.

Stone, D., Whalley, L. K., and Heard, D. E.: Tropospheric OH and HO_2 radicals: field measurements and model comparisons, Chem. Soc. Rev., 41, 6348-6404, https://doi.org/10.1039/c2cs35140d, 2012.

Taatjes, C. A., Welz, O., Eskola, A. J., Savee, J. D., Scheer, A. M., Shallcross, D. E., Rotavera, B., Lee, E. P. F., Dyke, J. M., Mok, D. K. W., Osborn, D. L., and Percival, C. J.: Direct measurements of conformer-dependent reactivity of the Criegee intermediate CH_3CHOO, Science, 340, 177-180, https://doi.org/10.1126/science.1234689, 2013.

Taatjes, C. A.: Criegee intermediates: what direct production and detection can teach us about

reactions of carbonyl oxides, Annu. Rev. Phys. Chem., 68, 183-207, https://doi.org/10.1146/annurev-physchem-052516-050739, 2017.

Valiev, R. R., Hasan, G., Salo, V. T., Kubečka, J., and Kurten, T.: Intersystem crossings drive atmospheric gas-phase dimer formation, J. Phys. Chem. A, 123, 6596-6604, https://doi.org/10.1021/acs.jpca.9b02559, 2019.

Wang, S., Riva, M., Yan, C., Ehn, M., and Wang, L.: Primary formation of highly oxidized multifunctional products in the OH-initiated oxidation of isoprene: a combined theoretical and experimental study, Environ. Sci. Technol., 52, 12255-12264, https://doi.org/10.1021/acs.est.8b02783, 2018.

Wang, S., Wu, R., Berndt, T., Ehn, M., and Wang, L.: Formation of highly oxidized radicals and multifunctional products from the atmospheric oxidation of alkylbenzenes, Environ. Sci. Technol., 51, 8442-8449, https://doi.org/10.1021/acs.est.7b02374, 2017.

Wennberg, P. O., Bates, K. H., Crounse, J. D., Dodson, L. G., McVay, R. C., Mertens, L. A., Nguyen, T. B., Praske, E., Schwantes, R. H., Smarte, M. D., Clair, J. M. S., Teng, A. P., Zhang, X., and Seinfeld, J. H.: Gas-phase reactions of isoprene and its major oxidation products, Chem. Rev., 118, 3337-3390, https://doi.org/10.1021/acs.chemrev.7b00439, 2018.

Winiberg, F. A. F., Dillon, T. J., Orr, S. C., Groß, C. B. M., Bejan, I., Brumby, C. A., Evans, M. J., Smith, S. C., Heard, D. E., and Seakins, P. W.: Direct measurements of OH and other product yields from the $HO_2 + CH_3C(O)O_2$ reaction, Atmos. Chem. Phys., 16, 4023-4042, https://doi.org/10.5194/acp-16-4023-2016, 2016.

Xu, L., Kollman, M. S., Song, C., Shilling, J. E., and Ng, N. L.: Effects of NO_x on the volatility of secondary organic aerosol from isoprene photooxidation, Environ. Sci. Technol., 48, 2253-2262, https://doi.org/10.1021/es404842g, 2014.

Xu, L., Møller, K. H., Crounse, J. D., Kjaergaard, H. G., and Wennberg, P. O.: New insights into the radical chemistry and product distribution in the OH-initiated oxidation of benzene, Environ. Sci. Technol., 54, 13467-13477, https://doi.org/10.1021/acs.est.0c04780, 2020.

Zhang, P., Wang, W., Zhang, T., Chen, L., Du, Y., Li, C., and Lv, J.: Theoretical study on the mechanism and kinetics for the self-reaction of $C_2H_5O_2$ radicals, J. Phys. Chem. A, 116, 4610-4620, https://doi.org/10.1021/jp301308u, 2012.

Zhao, Y., and Truhlar, D. G.: A new local density functional for main-group thermochemistry, transition metal bonding, thermochemical kinetics, and noncovalent interactions, J. Chem. Phys., 125, 194101-194119, https://doi.org/10.1063/1.2370993, 2006.

Zhao, Y., and Truhlar, D. G.: The M06 suite of density functionals for main group thermochemistry, thermochemical kinetics, noncovalent interactions, excited states, and transition elements: two new functionals and systematic testing of four M06-class functionals and 12 other functionals, Theor. Chem. Acc., 120, 215-241, https://doi.org/10.1007/s00214-007-0310-x, 2008.

Zheng, J., and Truhlar, D. G.: Direct dynamics study of hydrogen-transfer isomerization of 1-pentyl and 1-hexyl radicals, J. Phys. Chem. A, 113, 11919-11925, https://doi.org/10.1021/jp903345x, 2009.

Zheng, J., Xu, X., and Truhlar, D. G.: Minimally augmented Karlsruhe basis sets, Theor. Chem. Acc., 128, 295-305, https://doi.org/10.1007/s00214-010-0846-z, 2011.

Zhong, J., Kumar, M., Francisco, J. S., and Zeng, X. C.: Insight into chemistry on cloud/aerosol water surfaces, Acc. Chem. Res., 51, 1229-1237,

1016   https://doi.org/10.1021/acs.accounts.8b00051, 2018.

1017   Zhou, X., Liu, Y., Dong, W., and Yang, X.: Unimolecular reaction rate measurement of

1018   *syn*-CH$_3$CHOO, J. Phys. Chem. Lett., 10, 4817-4821,

1019   https://doi.org/10.1021/acs.jpclett.9b01740, 2019.

1020   Zhu, C., Kumar, M., Zhong, J., Li, L., Francisco, J. S., and Zeng, X. C.: New mechanistic

1021   pathways for Criegee-water chemistry at the air/water interface, J. Am. Chem. Soc., 138,

1022   11164-11169, https://doi.org/10.1021/jacs.6b04338, 2016.